Available online at www.sciencedirect.com
ScienceDirect
Journal of Sound and Vibration 302 (2007) 486–526
JOURNAL OF SOUND AND VIBRATION
www.elsevier.com/locate/jsvi

Novel schemes for inserting seismic dampers in shear-type systems based upon the mass proportional component of the Rayleigh damping matrix

T. Trombetti*, S. Silvestri

DISTART, Facoltà di Ingegneria, Università degli Studi di Bologna, Viale Risorgimento 2, 40136 Bologna, Italy

Received 1 April 2005; received in revised form 13 September 2006; accepted 8 November 2006
Available online 31 January 2007

Abstract

This paper presents the results of an extensive study carried out to investigate the applicability of a novel scheme for inserting added viscous dampers in shear-type systems. The findings, even though developed with specific reference to civil building structures, provide useful insight also for the effective addition of viscous dampers in mechanical dynamic systems (of similar characteristics) when excited at the base.

The novel scheme proposed (referred to as the MPD system) is based upon the mass proportional component of the Rayleigh damping matrix (MPD matrix) and is characterised by a peculiar damper placement which sees the dampers placed so that they connect each mass to a fixed point.

Firstly, the paper briefly recalls (a) the physical principles and (b) selected results of numerical investigations which show that the MPD system is characterised by superior dissipative properties.

Secondly, the paper investigates the implementation of the MPD system in civil building structures. Two solutions are envisaged herein: direct implementation (through the use of long buckling-resistant dampers which connect each storey to the ground) and indirect implementation (by placing common dampers between the structure and a very stiff lateral-resisting element adjacent or internal to the structure). The first solution leads to the implementation in the structure of an exact MPD matrix, if damper sizing is chosen appropriately. The second solution (simpler than the first one to implement in building structures) leads to an exact MPD matrix, if, in addition to appropriate damper sizing, the lateral-resisting element is infinitely stiff. As far as the direct implementation is concerned, this paper shows how long buckling-resistant braces are available for structural systems up to three storey high. As far as the indirect implementation is concerned, this paper shows (through extensive numerical parametric investigations) how this solution is capable of providing damping effects which are similar to those offered by the direct implementation, even for lateral-resisting elements characterised by finite lateral stiffness. The results obtained also provide insight for the optimal insertion of viscous dampers in coupled mechanical dynamic systems.

*Corresponding author. Tel.: +39 051 209 3242; fax: +39 051 209 3236.
E-mail addresses: tomaso.trombetti@mail.ing.unibo.it (T. Trombetti), stefano.silvestri@mail.ing.unibo.it (S. Silvestri).

0022-460X/$ - see front matter © 2007 Published by Elsevier Ltd.
doi:10.1016/j.jsv.2006.11.030

1. Introduction

Dissipative systems have widely proven their effectiveness in mitigating seismic effects in shear-type structures [1,2]. Still the issue is open in terms of identifying the additional damper system that maximises the overall dissipative properties of the structure under a wide range of dynamic inputs and with reference to a number of performance indexes [3–10].

In previous research works [11–17], the authors have examined the problem in an innovative, across the-board manner by studying damper placement and damper sizing contemporarily. This approach has led to the identification of a special scheme based upon the mass proportional damping (MPD) component of classic viscous damping matrices which is capable of maximising the overall dissipative properties of the structure under a wide range of dynamic inputs and with reference to a number of performance indexes. Sections 2–4 summarise the physical principles and the fundamental results of the previous research works carried out by the authors regarding the optimal damper insertion in shear-type systems. The interested reader may also refer to Refs. [11–17] for more detail information.

This special scheme (referred to as the MPD system) is characterised, among other properties, by a peculiar placement of the damping devices. Given the novelty of the proposed disposition (it differs considerably from the traditional interstorey damper setup), it is fundamental to develop a specific study of its applicability to actual building structures. Sections 5–7 report the results of these investigations. The parametric study is developed with specific reference to civil building structural systems, nonetheless the findings may give useful insight also into the effective addition of viscous dampers in coupled mechanical systems.

2. The dynamic system considered

The equations of motion of an N-degrees-of-freedom (N-dof) linear elastic dynamic system subjected to dynamic loading can be written, in time domain, as follows [18]:

$$\mathbf{M}\ddot{\mathbf{u}}(t) + \mathbf{C}\dot{\mathbf{u}}(t) + \mathbf{K}\mathbf{u}(t) = \mathbf{p}(t), \tag{1}$$

where $\mathbf{M}$ is the mass matrix, $\mathbf{K}$ the stiffness matrix, $\mathbf{C}$ the damping matrix, $\mathbf{u}(t)$ the displacement vector representing the displaced shape of the system and $\mathbf{p}(t)$ the vector of the externally applied dynamic loading. A dot over a symbol indicates differentiation with respect to time.

Let us consider a dynamic system composed of (i) an N-dof linear elastic shear-type system and (ii) a generic ensemble of added viscous dampers. Fig. 1a provides the physical representation typical of the mechanical engineering for the dynamic system considered, while Fig. 1b provides the physical representation typical of the structural engineering for the dynamic system considered. Internal (intrinsic) damping is neglected and a linear constitutive law of the type $F_d = cv$ (where F_d is the force provided by the damper, c is its damping coefficient and v is the relative velocity between the two damper ends) is assumed for the damping mechanism. It is well known that in this specific case:

- $\mathbf{u}(t) = \{u_1(t)\ u_2(t) \cdots u_N(t)\}^{\mathrm{T}}$ is the column vector of the mass displacements $u_i(t)$ of the shear-type system (with $i = 1,\ldots,N$ indicating the number of the masses from the left to the right in the case of the shear-type mechanical system and from the bottom to the top in the case of the shear-type structural system);
- the mass matrix is an $N \times N$ diagonal matrix, whose terms depend on the masses of the physical elements of the system [18];
- the stiffness matrix is an $N \times N$ banded (tri-diagonal) matrix, whose terms depend upon the stiffnesses of the physical elements of the system [18];
- the damping matrix is an $N \times N$ matrix which can be full, banded or diagonal depending on the ensemble of added viscous dampers which is introduced into the structure.

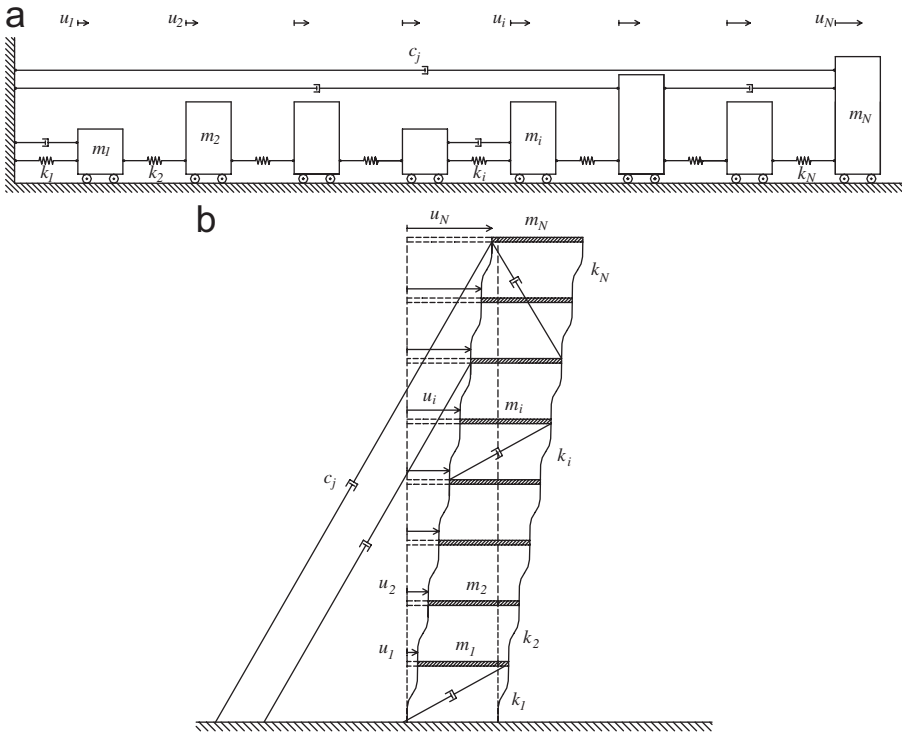

Fig. 1. (a) Physical representation of an N-dof shear-type mechanical system equipped with a generic system of added viscous dampers. (b) Physical representation of an N-dof shear-type structural system equipped with a generic system of added viscous dampers.

3. The MPD and SPD limiting cases of the Rayleigh damping matrix

Let us now consider an ensemble (system) of added viscous dampers which leads, for the generic N-storey linear elastic shear-type system described before, to a Rayleigh damping matrix $\mathbf{C}^R$ [18]. The Rayleigh damping matrix $\mathbf{C}^R$ has the following expression:

$$\mathbf{C}^R = \alpha\mathbf{M} + \beta\mathbf{K}, \tag{2}$$

where $\mathbf{M}$ and $\mathbf{K}$ are, respectively, the mass matrix and the stiffness matrix described in Section 2 and α and β are two constants having, respectively, units of s^{-1} and s.

Eq. (2) leads also to the definition of the following two limiting cases:

- Mass Proportional Damping matrix or MPD matrix:

$$\mathbf{C}^{\mathrm{MPD}} = \alpha\mathbf{M}. \tag{3}$$

- Stiffness Proportional Damping matrix or SPD matrix:

$$\mathbf{C}^{\mathrm{SPD}} = \beta\mathbf{K}. \tag{4}$$

Note that $\mathbf{C}^R = \mathbf{C}^{\mathrm{MPD}} + \mathbf{C}^{\mathrm{SPD}}$.

The system of added viscous dampers which leads to a damping matrix equal to a Rayleigh damping matrix is referred herein to as "*Rayleigh damping system*". Similarly, the system of added viscous dampers which

leads to a damping matrix equal to the MPD matrix is referred herein to as "*MPD system*" and the system of added viscous dampers which leads to a damping matrix equal to the SPD matrix is referred herein to as "*SPD system*".

Recalling the well-known form of the matrix **M** for a shear-type dynamic system leads to

$$\mathbf{C}^{\mathrm{MPD}} = \begin{bmatrix} \alpha m_1 & 0 & \dots & & & \dots & 0 \\ 0 & \alpha m_2 & 0 & \dots & & & \dots \\ \dots & 0 & \dots & & & & \\ & & & \alpha m_i & & & \\ & & & & \dots & & \dots \\ \dots & & & & & \alpha m_{N-1} & 0 \\ 0 & \dots & & & \dots & 0 & \alpha m_N \end{bmatrix}, \tag{5}$$

where m_i represents the mass of the ith element in the case of the shear-type mechanical system and the mass of the ith storey in the case of the shear-type structural system. By calling $\alpha m_i = c_i$ $(\forall i = 1, \dots, N)$, Eq. (5) becomes

$$\mathbf{C}^{\mathrm{MPD}} = \begin{bmatrix} c_1 & 0 & \dots & & & \dots & 0 \\ 0 & c_2 & 0 & \dots & & & \dots \\ \dots & 0 & \dots & & & & \\ & & & c_i & & & \\ & & & & \dots & & \dots \\ \dots & & & & & c_{N-1} & 0 \\ 0 & \dots & & & \dots & 0 & c_N \end{bmatrix}. \tag{6}$$

From simple kinematics considerations and from the definition of element c_{rs} of a generic damping matrix, it can be observed that the damping matrix provided by Eq. (6) corresponds to a physical system of added viscous dampers, which connect each storey to a fixed point (e.g. the ground). In detail, with reference to the definition of c_{rs} (the force corresponding to coordinate r due to unit velocity of coordinate s) and to the form of Eq. (6), a unit velocity along coordinate i, $\dot{u}_i = 1$, produces only a damping force of magnitude $F_i = c_i \dot{u}_i = c_i 1 = c_i$ along the direction of coordinate i: this can be physically achieved only by placing dampers which connect each ith storey to a fixed point (e.g. the ground).

Similarly, recalling the well-known form of the matrix **K** for a shear-type dynamic system leads to

$$\mathbf{C}^{\mathrm{SPD}} = \begin{bmatrix} \beta k_1 + \beta k_2 & -\beta k_2 & 0 & \dots & & & 0 \\ -\beta k_2 & \beta k_2 + \beta k_3 & -\beta k_3 & 0 & \dots & & \dots \\ 0 & -\beta k_3 & \beta k_3 + \beta k_4 & \dots & & & \\ \dots & & \dots & \dots & & & \\ & & & & \dots & \dots & 0 \\ \dots & & & & \dots & \beta k_{N-1} + \beta k_N & -\beta k_N \\ 0 & \dots & & & & -\beta k_N & \beta k_N \end{bmatrix}, \tag{7}$$

where k_i represents the stiffness connecting the ith element to the $(i-1)$th element (i.e. to the fixed point if $i = 1$) in the case of the shear-type mechanical system and the total lateral stiffness of the vertical elements connecting the ith storey to the $(i-1)$th storey (i.e. to the ground if $i = 1$) in the case of the shear-type

structural system. By calling $\beta k_i = c_i$ ($\forall i = 1, \ldots, N$), Eq. (7) becomes

$$\mathbf{C}^{\mathrm{SPD}} = \begin{bmatrix} c_1 + c_2 & -c_2 & 0 & \ldots & & & 0 \\ -c_2 & c_2 + c_3 & -c_3 & 0 & \ldots & & \ldots \\ 0 & -c_3 & c_3 + c_4 & \ldots & & & \\ \ldots & & \ldots & \ldots & & & \\ & & & & \ldots & \ldots & 0 \\ \ldots & & & & \ldots & c_{N-1} + c_N & -c_N \\ 0 & \ldots & & & & -c_N & c_N \end{bmatrix}. \tag{8}$$

It can be then observed that the damping matrix provided by Eq. (8) corresponds to a physical system of added viscous dampers placed so that they connect adjacent storeys. In detail, with reference to the definition of c_{rs} and to the form of Eq. (8), a unit velocity along coordinate i, $\dot{u}_i = 1$, produces:

- a positive damping force of magnitude $F_i = (c_i + c_{i+1})\dot{u}_i = (c_i + c_{i+1})1 = c_i + c_{i+1}$ along the direction of coordinate i;
- a negative damping force of magnitude $F_{i-1} = -c_i\dot{u}_i = -c_i 1 = -c_i$ along the direction of coordinate $(i-1)$;
- a negative damping force of magnitude $F_{i+1} = -c_{i+1}\dot{u}_i = -c_{i+1}1 = -c_{i+1}$ along the direction of coordinate $(i+1)$.

From simple kinematics considerations, it can be seen that this can be physically achieved only by placing dampers so that they connect adjacent storeys. Damper characterised by coefficient c_i (as defined with respect to the motion of coordinates i and $(i+1)$) connects storey i (or coordinate i) to storey $(i-1)$ (or coordinate $(i-1)$). Damper characterised by coefficient c_{i+1} connects storey i (or coordinate i) to storey $(i+1)$ (or coordinate $(i+1)$).

Consequently, the Rayleigh damping matrix given by Eq. (2) corresponds to a physical system which encompasses both added viscous dampers connecting each storey to the ground and added viscous dampers connecting adjacent storeys.

With reference to the illustrative 3-dof shear-type mechanical system represented in Fig. 2a:

- when a Rayleigh system is inserted into the shear-type system, the physical system thus obtained corresponds to that schematically represented in Fig. 2b;
- when an MPD system is inserted into the shear-type system, the physical system thus obtained corresponds to that schematically represented in Fig. 2c;
- when an SPD system is inserted into the shear-type system, the physical system thus obtained corresponds to that schematically represented in Fig. 2d.

With reference to the illustrative 3-dof shear-type structural system represented in Fig. 2e:

- when a Rayleigh system is inserted into the shear-type system, the physical system thus obtained corresponds to that schematically represented in Fig. 2f;
- when an MPD system is inserted into the shear-type system, the physical system thus obtained corresponds to that schematically represented in Fig. 2g;
- when an SPD system is inserted into the shear-type system, the physical system thus obtained corresponds to that schematically represented in Fig. 2h.

Inspection of Figs. 2c, d, g and h indicates that the MPD and the SPD systems are physically separated. Inspection of Figs. 2c, d, g and h also allows to formulate the following alternative definitions in terms of damper placement and damper sizing for the MPD and the SPD systems (see also details given in Refs. [11–17]):

- *MPD system*: the dampers are placed in such a way as to connect each mass to a fixed point. This placement can be referred to as *"Fixed Point placement"* or *"FP-placement"*. The dampers are sized so that each

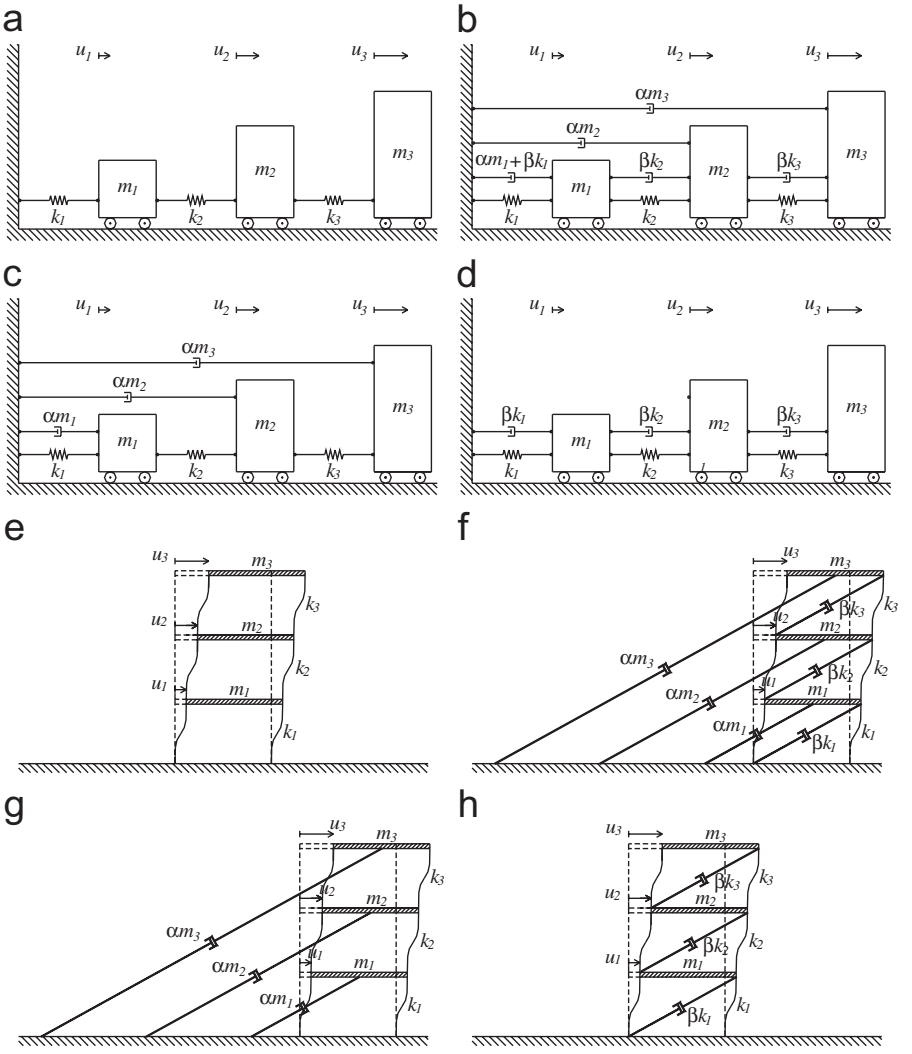

Fig. 2. A 3-dof shear-type mechanical system: (a) undamped, (b) equipped with Rayleigh damping system, (c) equipped with MPD system and (d) equipped with SPD system. A 3-dof shear-type structural system: (e) undamped, (f) equipped with Rayleigh damping system, (g) equipped with MPD system and (h) equipped with SPD system.

damping coefficient c_j is proportional to the corresponding mass m_j. This sizing can be referred to as *''Mass Proportional sizing''* or *''MP-sizing''*.

- *SPD system*: the dampers are placed in such a way as to connect two adjacent masses. This placement can be referred to as *''Inter-Storey placement''* or *''IS-placement''*. The dampers are sized so that each damping coefficient c_j is proportional to the stiffness k_j connecting these two adjacent masses. This sizing can be referred to as *''Stiffness Proportional sizing''* or *''SP-sizing''*.

4. Performances of the MPD and SPD systems

As illustrative examples of the performances provided by the MPD and SPD systems (and, more in general, of the performances provided by damper systems characterised by FP-placement and IS-placement), analytical findings and selected numerical results are presented in the following.

4.1. The equal "total size" constraint

In order to make meaningful comparisons of the dissipative performances offered by different damper systems, the following condition (referred to as the equal "total size" constraint) is imposed upon their "total size". The sum, c_{tot}, of the damping coefficients, c_j, of all M added viscous dampers introduced into the shear-type system, is equal to a set value, $\bar{c}$, as given by the following formula:

$$c_{\text{tot}} = \sum_{j=1}^{M} c_j = \bar{c}. \tag{9}$$

In accordance with the usual matrix notation, where c_{rs} is the rsth element of the system damping matrix $\mathbf{C}$, for N-dof shear-type systems, this condition translates into

$$\sum_{r=1}^{N} \sum_{s=r}^{N} c_{rs} = \bar{c}. \tag{10}$$

4.2. Physical dissipative properties of the Rayleigh damping systems and its limiting cases

All results presented in this section are obtained with reference to the class of shear-type systems characterised by values of mass and stiffness which do not vary ($m_i = m$ and $k_i = k$, $\forall i = 1, \ldots, N$).

For the class of shear-type systems here considered, imposing the equal "total size" constraint to a generic Rayleigh damping system leads to the identification of a class of Rayleigh damping systems characterised by the following specific values $\bar{\alpha}^R$ and $\bar{\beta}^R$ of the α and β parameters:

$$\begin{aligned} \bar{\alpha}^R &= \bar{\alpha}(1-\gamma), \\ \bar{\beta}^R &= \bar{\beta}\gamma, \end{aligned} \tag{11}$$

where

- γ is a dimensionless parameter with values ranging between 0 and 1, that identifies each specific Rayleigh system within the class defined above;
- $$\bar{\alpha} = \frac{\bar{c}}{Nm} = \frac{c_0}{m}, \tag{12}$$
- $$\bar{\beta} = \frac{\bar{c}}{Nk} = \frac{c_0}{k}, \tag{13}$$
- $$c_0 = \frac{\bar{c}}{N}, \tag{14}$$

$\gamma = 0$ identifies the MPD system, whilst $\gamma = 1$ identifies the SPD system.

Note that:

- for N-dof shear-type systems, the MPD and the SPD systems are characterised by $M = N$;
- for the MPD system:

$$\begin{aligned} \bar{\alpha}^{\text{MPD}} &= \bar{\alpha}, \\ \bar{\beta}^{\text{MPD}} &= 0, \end{aligned} \tag{15}$$

- for the SPD system:

$$\begin{aligned} \bar{\alpha}^{\text{SPD}} &= 0, \\ \bar{\beta}^{\text{SPD}} &= \bar{\beta}, \end{aligned} \tag{16}$$

- the MPD and the SPD systems are made up of N equally sized dampers (each one characterised by c_0).

Note that Eqs. (12) and (13) lead to the following relationship between the $\bar{\alpha}$ and $\bar{\beta}$ values that guarantees the satisfaction of the equal "total size" constraint, independently of $\bar{c}$:

$$\bar{\alpha} = \bar{\beta}\omega_0^2 \tag{17}$$

where $\omega_0 = \sqrt{k/m}$ is a useful reference circular frequency that corresponds to the circular frequency of a single-degree-of-freedom (sdof) system with stiffness equal to k and mass equal to m.

For classically damped N-dof dynamic systems, it is possible to define a damping ratio for each mode of vibration [18]. For Rayleigh damped N-dof dynamic systems, it is well known that the ith modal damping ratio, ξ_i^R, expressed according to the notation of Eq. (2), is given by

$$\xi_i^R(\omega_i) = \frac{\alpha}{2\omega_i} + \frac{\beta\omega_i}{2}, \tag{18}$$

where ω_i is the ith modal (undamped) circular frequency of the N-dof dynamic system.

For the class of shear-type systems here considered, imposing to Eq. (18) the equal "total size" constraint in the form of Eqs. (15), (16), (11) and (17) leads to

$$\xi_i^{\mathrm{MPD}} = \frac{\bar{\alpha}}{2\omega_i} = \frac{\bar{\alpha}}{2\omega_0}\left(\frac{\omega_0}{\omega_i}\right) = \frac{\xi_0}{\Omega_i}, \tag{19}$$

$$\xi_i^{\mathrm{SPD}} = \frac{\bar{\beta}\omega_i}{2} = \frac{\bar{\alpha}\omega_i}{2\omega_0^2} = \frac{\bar{\alpha}}{2\omega_0}\left(\frac{\omega_i}{\omega_0}\right) = \xi_0\Omega_i, \tag{20}$$

$$\begin{aligned}\xi_i^R &= \frac{\bar{\alpha}^R}{2\omega_i} + \frac{\bar{\beta}^R\omega_i}{2},\\ &= \frac{\bar{\alpha}}{2\omega_i}(1-\gamma) + \frac{\bar{\beta}\omega_i}{2}\gamma,\\ &= \xi_i^{\mathrm{MPD}}(1-\gamma) + \xi_i^{\mathrm{SPD}}\gamma,\\ &= \xi_i^{\mathrm{MPD}} - \gamma(\xi_i^{\mathrm{MPD}} - \xi_i^{\mathrm{SPD}}),\end{aligned} \tag{21}$$

where

- $\Omega_i = \omega_i/\omega_0$ is the ith normalised circular frequency (with respect to the reference circular frequency ω_0);
- $\xi_0 = \frac{\bar{\alpha}}{2\omega_0} = \frac{\bar{\beta}}{2}\omega_0 = \frac{\bar{c}}{2N\sqrt{km}} = \frac{c_0}{2\sqrt{km}}$, is a reference damping ratio that only depends on the characteristics of the shear-type system (k, m and N) and the "total size" ($\bar{c}$) of the damper system. It is worth pointing out that ξ_0 corresponds to the damping ratio of an sdof system with stiffness equal to k, mass equal to m and damper coefficient equal to c_0.

Fig. 3 shows the modal damping ratio vs. normalised circular frequency curves for a shear-type system equipped with the MPD system, the SPD system and the Rayleigh damping system characterised by $\gamma = 0.5$, as obtained under the equal "total size" constraint. As known, MPD systems provide a modal damping ratio which progressively (hyperbolically) decreases as the modal frequency gets higher and higher; while SPD systems provide a modal damping ratio which linearly increases as the modal frequency gets higher and higher. Note that, as per Eq. (21), the Rayleigh damping system is characterised by intermediate properties.

In order to draw conclusions regarding the relative dissipative efficiencies of the MPD and the SPD systems, it is necessary to know whether the normalised circular frequencies Ω_i of the modes of vibration which govern the response of the dynamic system considered are larger or smaller than unity.

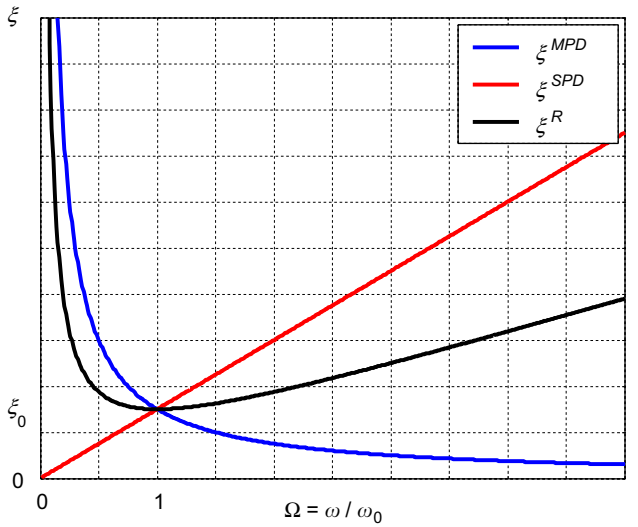

Fig. 3. The modal damping ratio vs. normalised circular frequency curves for a dynamic system equipped with the MPD system (blue line), the SPD system (red line) and the Rayleigh damping system characterised by $\gamma = 0.5$ (black line), as obtained under the equal "total size" constraint.

From Eqs. (19) and (20), it can be deduced that

$$\frac{\xi_i^{\mathrm{SPD}}}{\xi_j^{\mathrm{MPD}}} = \Omega_i \Omega_j. \tag{22}$$

Specialising Eq. (22) for $i = j$, it is clear that:

- if $\Omega_i = 1$ then $\xi_i^{\mathrm{MPD}} = \xi_0 = \xi_i^{\mathrm{SPD}}$;
- if $\Omega_i < 1$ then $\xi_i^{\mathrm{MPD}} > \xi_0 > \xi_i^{\mathrm{SPD}}$;
- if $\Omega_i > 1$ then $\xi_i^{\mathrm{MPD}} < \xi_0 < \xi_i^{\mathrm{SPD}}$.

Specialising Eq. (22) for $i = j = 1$ leads to

$$\frac{\xi_1^{\mathrm{SPD}}}{\xi_1^{\mathrm{MPD}}} = \Omega_1^2. \tag{23}$$

For the class of shear-type systems here considered, investigation of the properties of the normalised circular frequencies Ω_i $(i = 1, \ldots, N)$, which involves the study of the eigenproblem of a banded and an identity matrices, reveals that the following result is demonstrated [17]:

$$\Omega_1 < 1, \tag{24}$$

which, thanks to Eq. (23), directly leads to

$$\frac{\xi_1^{\mathrm{SPD}}}{\xi_1^{\mathrm{MPD}}} < 1 \tag{25}$$

i.e., the insertion into the shear-type (either mechanical or structural) system of an MPD system leads to a damping ratio of the fundamental mode of vibration which is always larger than that given by the insertion of an equal "total size" SPD system ($\xi_1^{\mathrm{MPD}} > \xi_1^{\mathrm{SPD}}$). Also from Eq. (21) it is clear that the insertion into the shear-type (either mechanical or structural) system of an MPD system leads to a damping ratio of the fundamental mode of vibration which is larger than that given by the insertion of any Rayleigh damping system of equal "total size". This result is of fundamental importance for shear-type systems characterised by dynamic

response governed by the first mode of vibration, such as those excited at the base with a broad-band excitation (such as the earthquake input).

Still, the study of the properties of the first normalised circular frequency Ω_1 reveals that the following results are demonstrated [17]:

$$\xi_1^{\mathrm{MPD}} > \xi_0\sqrt{N}, \tag{26}$$

$$\xi_1^{\mathrm{SPD}} < \frac{\xi_0}{\sqrt{N}}, \tag{27}$$

$$\frac{\xi_1^{\mathrm{SPD}}}{\xi_1^{\mathrm{MPD}}} < \frac{1}{N}, \tag{28}$$

which indicate that the superior dissipative properties of the MPD system with respect to those of the equal "total size" SPD system increase with increasing number of degrees of freedom N.

Fig. 4 shows the numerical values of the ratio $\xi_1^{\mathrm{SPD}}/\xi_1^{\mathrm{MPD}}$ for N varying from 2 to 30, as obtained for the class of shear-type systems here considered. The figure also shows the curve $y = 1/N$ which, as demonstrated in Ref. [17], represents an upper bound for $\xi_1^{\mathrm{SPD}}/\xi_1^{\mathrm{MPD}}$.

Focusing on higher modes of vibration, the study of the properties of Ω_i $(i = 1, \ldots, N)$ reveals that also the following result is demonstrated [17]:

$$\xi_1^{\mathrm{MPD}} > \xi_{N-p+1}^{\mathrm{SPD}} > \xi_{N-p}^{\mathrm{SPD}} > \cdots > \xi_1^{\mathrm{SPD}}, \tag{29}$$

where p is the number of modes of vibrations for which $\Omega_i \leqslant 1$ $(i = 1, \ldots, p)$. It is numerically seen [17] that

$$p = \left[\frac{N+2}{3}\right], \tag{30}$$

where $[z]$ indicates the integer part of z.

Fig. 5 shows the numerical values of the ratio between $N - p + 1$ and N, as obtained for the class of shear-type systems here considered. Inspection of this figure indicates that ξ_1^{MPD} is larger than roughly the first 70% (with respect to the total number of modal damping ratios) modal damping ratios ξ_i^{SPD}.

All above results clearly indicate that a shear-type (either mechanical or structural) system equipped with added viscous dampers which lead to an MPD matrix, when excited at the base with a broad-band excitation (such as the earthquake input), should always display superior dissipative properties than those displayed by

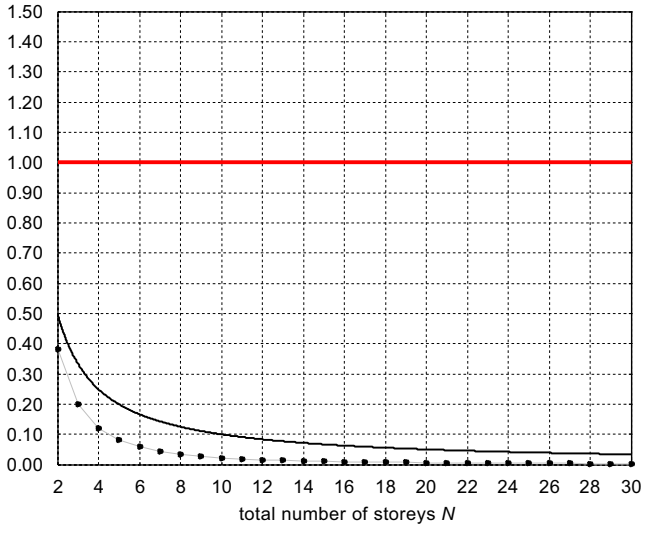

Fig. 4. The ratio $\xi_1^{\mathrm{SPD}}/\xi_1^{\mathrm{MPD}}$ (black dots) and its upper bound $y = 1/N$ (black continuous line) for N varying from 2 to 30. The red line indicates the curve $y = 1$.

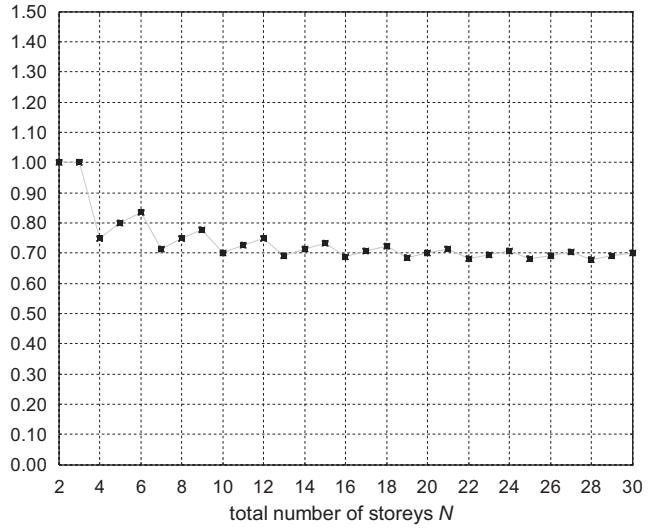

Fig. 5. The $(N-p+1)/N$ ratio (black squares) for N varying from 2 to 30.

a shear-type system equipped with equal "total size" added viscous dampers which lead to an SPD matrix. Also, these superior dissipative properties should increase with increasing number of degrees of freedom.

Finally, as far as the geometrical sum of the modal damping ratios, $\xi_{\text{g.s.}} = \sqrt{\sum_{i=1}^{N} \xi_i^2}$, is concerned, it is demonstrated that [17]

$$\frac{\xi_{\text{g.s.}}^{\text{SPD}}}{\xi_{\text{g.s.}}^{\text{MPD}}} = \frac{\sqrt{\sum_{i=1}^{N} (\xi_i^{\text{SPD}})^2}}{\sqrt{\sum_{i=1}^{N} (\xi_i^{\text{MPD}})^2}} = \sqrt{\frac{4N-2}{N^2+N}}. \tag{31}$$

For shear-type systems subjected to a broad-band base excitation and under the here conservative (pejorative with respect to the evaluation of the damping performances of shear-type systems equipped with the MPD system) hypothesis that all modes have the same importance in the determination of the global system response, the geometrical sum of the damping ratios can be reasonably assumed as a meaningful performance index of the dissipative effects of the MPD and SPD systems. Therefore, Eq. (31) indicates that the dissipative effects of the MPD system are larger than those of the equal "total size" SPD system even for $N>2$ and that they increase for increasing N, as also illustrated in Fig. 6.

4.3. Numerical verifications of the dissipative properties of the MPD and SPD systems

This section presents selected numerical results which synthesise the findings of extensive parametric analyses carried out by the authors [11–17], aimed at comparing the dissipative properties of MPD systems with those of other generic (classical and nonclassical) damping systems.

Specific reference is now made to civil building structures equipped with additional viscous damping devices. However, the results that will be obtained may be easily extended to mechanical systems of similar characteristics.

Firstly, this section presents results (in terms of floor responses and damper forces) obtained for Rayleigh damping systems. Secondly, the dissipative properties of the MPD and the SPD systems will be compared with those of other "optimised" (in their damping efficiency) systems of added viscous dampers obtained using numerical algorithms.

All results are developed with reference to the 6-storey shear-type structural system of Fig. 7a, which is characterised by values of mass and lateral stiffness which do not vary along the building height. At each

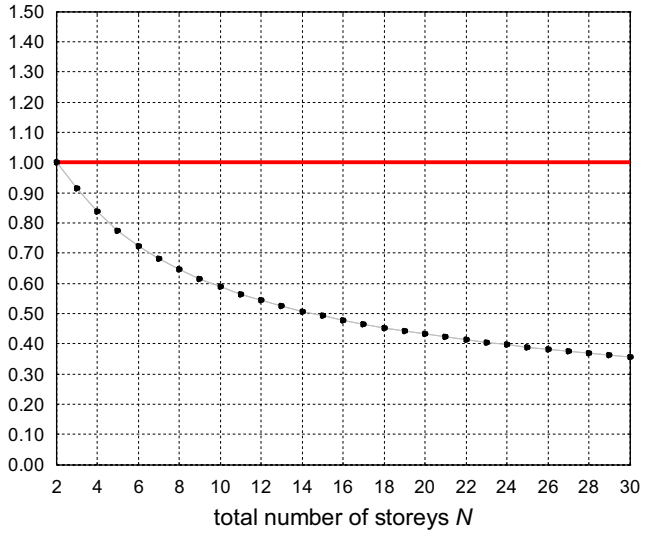

Fig. 6. $\xi_{\text{g.s.}}^{\text{SPD}}/\xi_{\text{g.s.}}^{\text{MPD}}$ (black dots) for N varying from 2 to 30.

storey, the lateral stiffness[1] of the vertical elements connecting one floor to the adjacent one is equal to $k_i = k = 4 \times 10^7\,\text{N/m}$ and the floor mass (see footnote 1) is equal to $m_i = m = 0.8 \times 10^5\,\text{kg}$. Interstorey height is equal to 3.0 m. The periods of vibration of the structure are given in Table 1. Internal damping is neglected and the set (see footnote 1) value $\bar{c}$ considered herein is equal to $9.0 \times 10^6\,\text{N s/m}$.

As far as Rayleigh damping systems are only concerned, Fig. 8 shows σ_i as functions of parameter γ. σ_i being the square root of the mean square response [19] (that coincides with the standard deviation for stochastic inputs with zero mean value), of the ith storey displacement of the structure subjected at the base to a white noise acceleration. The white noise considered has the following characteristics: band-limited between 0 and $\bar{\omega} = 60\,\text{rad/s}$, stationary, Gaussian with zero mean and characterised by constant power spectral density of amplitude $A^2 = 0.144\,\text{m}^2/\text{s}^3$.[2]

Inspection of Fig. 8 shows that, among all Rayleigh damping systems, the MPD system (characterised by $\gamma = 0$ and represented in Fig. 7b) represents the optimum solution as far as minimising σ_i is concerned, whilst the SPD system (characterised by $\gamma = 1$ and represented in Fig. 7c) provides the worst solution. The curves $\sigma_i(\gamma)$ of Fig. 8 are extremely smooth and feature an almost horizontal tangent at $\gamma = 0$, so that systems characterised by γ values close but not equal to zero still show very low values for σ_i. This clearly indicates the "robustness" of the dissipation efficiency of MPD systems.

Note that, under the equal "total size" constraint, given that, for the structure examined, $m_i = m$ and $k_i = k$, $\forall i = 1, \ldots, 6$, it turns out that all dampers are equal in size for both MPD and SPD systems ($c_j = \bar{c}/6 = 1.5 \times 10^6\,\text{N s/m}$, $\forall j$). Therefore, the only difference between these two systems is the actual placement of the viscous devices. The results of Fig. 8 thus highlight the prime importance of damper placement to achieving dissipative effectiveness. Basically, in the class of structures characterised by a Rayleigh damping system, the conventional arrangement of dampers between adjacent storeys (characteristic of the SPD system) is that which provides least dissipation efficiency. On the other hand, dampers placed in such a way as to connect each storey to a fixed point, typical of the MPD system proposed herein, provide maximum damping efficiency.

Fig. 9 shows the sum, Σ, of the standard deviations of the forces exerted through all dampers (under the stochastic white noise acceleration of above) as function of parameter γ. Inspection of this figure clearly indicates that, from an engineering point of view, the sum of the forces exerted through all dampers is

[1]These specific values k, m and $\bar{c}$ are selected for the sake of comparison with other research results regarding the optimal placement of added viscous dampers that are available in literature [3].

[2]These values have been chosen so that standard deviation of acceleration at the base of the structure supplied by this stochastic process is equal to $0.3g$.

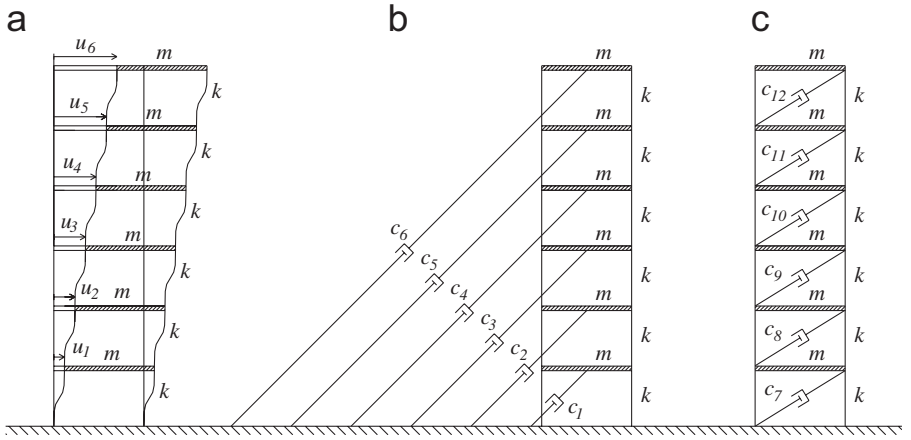

Fig. 7. The reference 6-storey shear-type structure: (a) as it is, (b) equipped with the MPD system and (c) equipped with the SPD system.

Table 1
Periods of vibration of the reference structure (s)

T_1	T_2	T_3	T_4	T_5	T_6
1.166	0.396	0.247	0.188	0.159	0.145

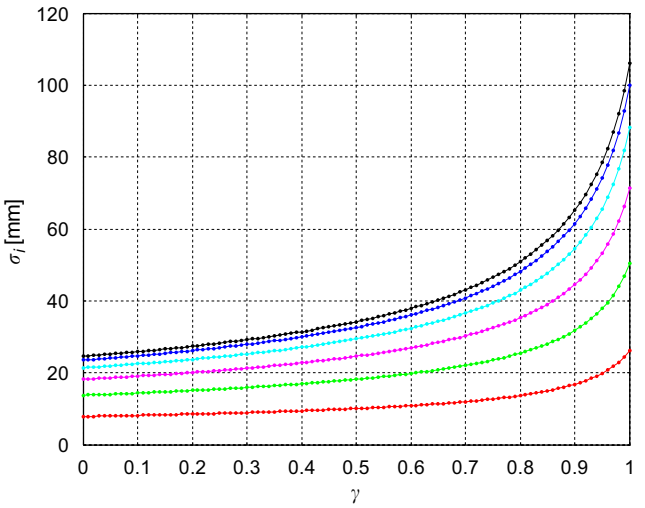

Fig. 8. σ_i vs. γ curves for the reference 6-storey shear-type structure: $i = 1$ (red), $i = 2$ (green), $i = 3$ (magenta), $i = 4$ (cyan), $i = 5$ (blue), $i = 6$ (black).

substantially the same for all damper systems and, therefore, the superior performances offered by the MPD system with respect to the SPD system do not come at the expense of larger forces exerted through the dampers, but are due to its intrinsic physical properties [17] recalled in Section 4.2.

As far as nonclassical damping systems are concerned, Fig. 10 shows the σ_i profiles as obtained for the reference structure equipped with the following systems of added viscous dampers (all obtained under the equal "total size" constraint):

- SPD system;
- TAK system;

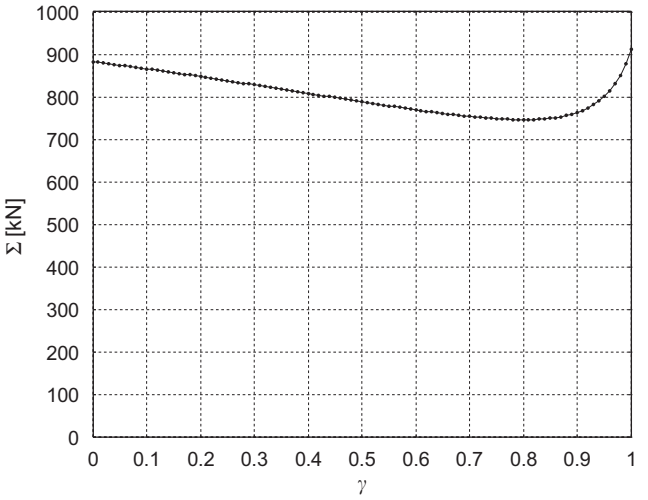

Fig. 9. Sum, Σ, of the standard deviations of the forces exerted through all dampers (under stochastic input) as a function of parameter γ for the reference 6-storey shear-type structure.

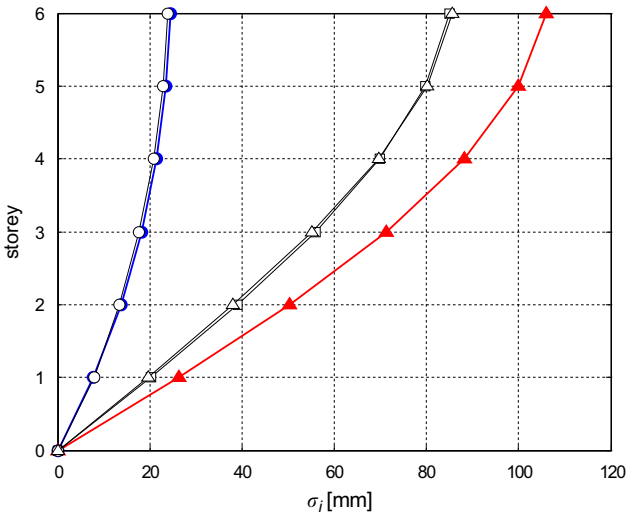

Fig. 10. Standard deviations of storey responses, σ_i, for the reference 6-storey shear-type structure equipped with the (—▲—, red) SPD, (—△—) TAK, (—□—) GIOIS, (—●—, blue) MPD and (—○—) GIOFP systems.

- GIOIS system;
- MPD system;
- GIOFP system;
- GIOFREE system.

The TAK system is identified as "optimal" in the research works of Izuru Takewaki [3]. This system is characterised by an IS-placement. The size of the dampers is determined through inverse problem approach so that the sum of amplitudes of the transfer functions of interstorey drifts evaluated at the undamped fundamental natural frequency is minimised.

The GIOIS, GIOFP and GIOFREE systems are identified as "optimal" making use of genetic algorithms [9,20–26], as already done in previous research works carried out by the authors [15,16]. The basic characteristics of the GA here adopted can be summarised as follows:

- population: 30 individuals;
- mutation choice: 18%;
- elitism choice: 18%;
- number of iteration: 150.

The GIOIS is the system characterised by "optimal" sizing for the IS-placement.

The GIOFP is the system characterised by "optimal" sizing for the FP-placement.

The GIOFREE system is obtained imposing no constraint upon damper placement so that all possible damper positions can be considered (i.e. dampers may connect adjacent storeys, nonadjacent storeys and storeys to a fixed point). The size of the dampers is determined in order to minimise the average of the standard deviations of the interstorey drift angles of the structure subjected to the white noise input acceleration described before [15,16].

Table 2 provides the values of the damping coefficients for the various damping systems considered with reference to the notation of Fig. 7.

Note that the GIOFP and the GIOFREE systems are identical. This is a further indication that FP-placement is capable of providing superior dissipative properties. In the next part of this section, reference will be made to the GIOFP system only.

Inspection of Fig. 10 shows that both the systems characterised by an FP-placement (MPD and GIOFP) lead to storey responses which are much smaller (up to 4 times) than those obtained for systems characterised by an IS-placement (SPD, TAK and GIOIS).

Fig. 11 shows the averages, μ_{Σ}, over 40 historically recorded earthquake ground motions all scaled to the same peak ground acceleration (PGA) of $0.3g$ (where g represents the gravity acceleration), of the sums of the maximum forces exerted through all dampers as obtained for the reference structure equipped with the following systems of added viscous dampers: SPD, TAK, GIOIS, MPD and GIOFP systems.

Inspection of this figure clearly indicates that, again, from an engineering point of view, the sum of the forces exerted through all dampers is substantially the same for all damper systems and, therefore, the superior performances offered by the MPD system (and, in general, by systems characterised by FP-placement) with respect to the SPD system (and, in general, to systems characterised by traditional IS-placement) do not come at the expense of larger forces exerted through the dampers, but are due to its intrinsic physical properties [17] recalled in Section 4.2.

Basically, the selected results here presented illustrate how systems characterised by the innovative fixed-point damper placement (as it is the case of the MPD system) leads to damping efficiency which is far superior

Table 2
Values of the damping coefficients ($\times 10^6$ N s/m) for the various damping systems considered with reference to the notation of Fig. 7

	SPD	TAK	GIOIS	MPD	GIOFP	GIOFREE
c_1	—	—	—	1.5	1.02	1.02
c_2	—	—	—	1.5	1.53	1.53
c_3	—	—	—	1.5	1.70	1.70
c_4	—	—	—	1.5	1.70	1.70
c_5	—	—	—	1.5	1.53	1.53
c_6	—	—	—	1.5	1.53	1.53
c_7	1.5	4.80	3.79	—	—	0
c_8	1.5	4.20	3.32	—	—	0
c_9	1.5	0	1.89	—	—	0
c_{10}	1.5	0	0	—	—	0
c_{11}	1.5	0	0	—	—	0
c_{12}	1.5	0	0	—	—	0

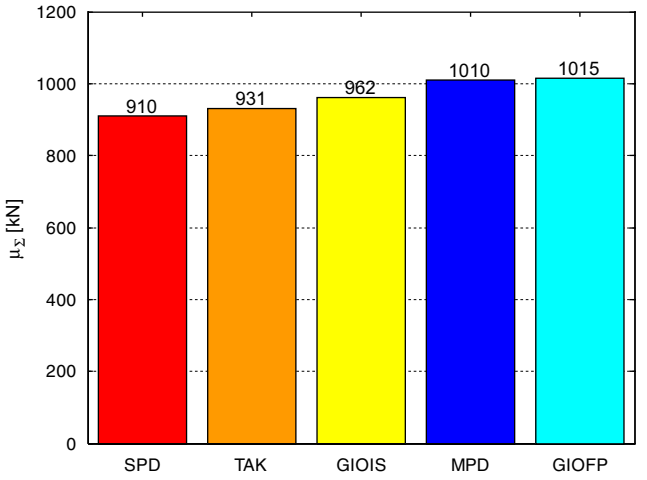

Fig. 11. Averages, μ_Σ, (over 40 historically recorded earthquake ground motions all scaled to a PGA value of $0.3g$) of the sums of maximum forces exerted through all dampers for the reference 6-storey shear-type structure equipped with the SPD (red), TAK (orange), GIOIS (yellow), MPD (blue) and GIOFP (cyan) systems.

to that offered by the traditional damper placements which see dampers placed between adjacent storeys (as it is the case of the SPD system).

5. Applicability of the MPD systems

As recalled in the previous section, the MPD system and, in general, damper systems characterised by FP-placement, lead to good damping performances. However, the issue of how to implement FP-placement in real shear-type systems still needs to be addressed.

In the following analyses, MPD systems will be taken as reference of the performances offered by the class of damper systems characterised by FP-placement (Figs. 12a, b, d and e) and SPD systems will be taken as reference of the performances offered by the class of damper systems characterised by IS-placement (Figs. 12c and f).

With reference to the schematic representation of Figs. 12a and d, a "direct implementation" of the MPD system (that leads to a damping matrix which corresponds to an exact MPD matrix, if damper sizing is chosen appropriately) can be obtained using the ground as fixed point. This is achieved by placing dampers so that they connect each mass to the ground.

With reference to the schematic representation of Figs. 12b and e, an "indirect implementation" of the MPD system can be obtained using a "support" shear-type system as fixed point. This is achieved by placing dampers so that they connect the shear-type system to be damped ("reference" shear-type system) to a "support" shear-type system (which must be characterised by a large, ideally infinite, stiffness).

6. Direct implementation of the MPD systems

For shear-type mechanical systems, the direct implementation of the MPD system should pose no problems if enough space is available.

For shear-type structural systems, in order to obtain a direct implementation of the MPD systems, it is necessary to introduce dissipative braces of considerable length. At the present time, the following technological solutions can be envisaged to overcome the length problem:

- use of the so-called "mega braces" of the Taylor Devices Company, already employed (though not following an exact MPD scheme) for the Chapultepec Tower (best known as Torre Major and shown in Fig. 13) in Mexico City. In this building, the dampers connect floors which are 2 storeys apart;

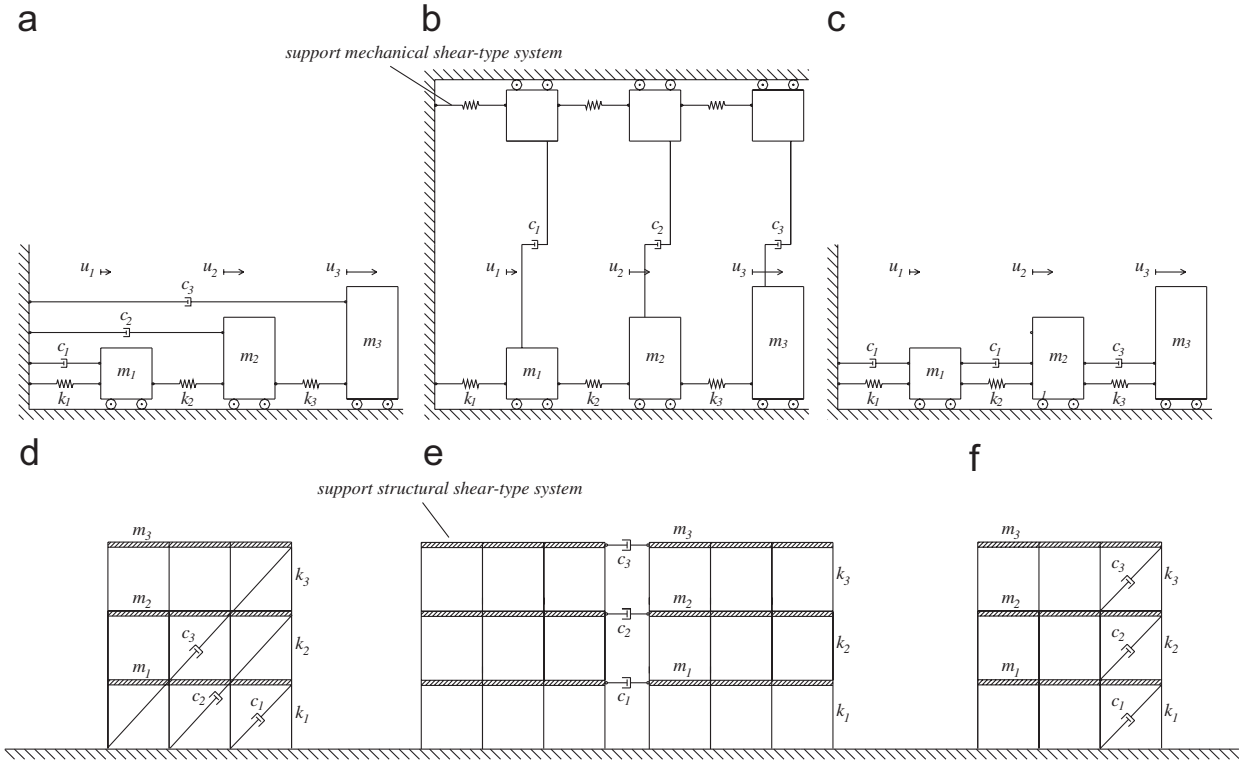

Fig. 12. Shear-type mechanical system: (a) fixed point placement obtained through direct implementation, (b) fixed point placement obtained through indirect implementation and (c) interstorey placement. Shear-type structural system: (d) fixed point placement obtained through direct implementation, (e) fixed point placement obtained through indirect implementation and (f) interstorey placement.

- use of the so-called "unbonded braces" [27] of the Nippon Steel Corporation, already employed (though not following an exact MPD scheme) for the Osaka International Conference Centre [28], shown in Fig. 14a, and the retrofit of the Wallace F. Bennett Federal Building in Salt Lake City [29], shown in Fig. 14b;
- use of prestressed steel cables coupled with silicon dampers as proposed in the SPIDER European research project [30] whose schematic representation can be seen in Fig. 15.

In both the Chapultepec Tower and the Osaka International Conference Centre, the dampers connect floors which are 2 or 3 storeys apart and therefore the up to date technology is readily available to successfully implement direct MPD systems for building structures up to 3 storeys high.

It must be noticed that, for civil building structures, direct implementation requires specific building details to be studied and addressed which may prove to be expensive (such as the long connections for the bracing system and the passage of the bracing system through the floors).

7. Indirect implementation of the MPD systems

For both shear-type mechanical and structural systems, indirect implementation should be deeply investigated in order to assess if it is capable of providing damping effects which are similar to those offered by the direct implementation. Without loss of generality, the following parametric study is carried out with specific reference to shear-type structural systems, nonetheless all the results may be easily extended to shear-type mechanical systems.

Indirect implementation of the MPD system does not require specific dampers and expensive building details, but simply places traditional viscous dampers so that they connect the reference structure to

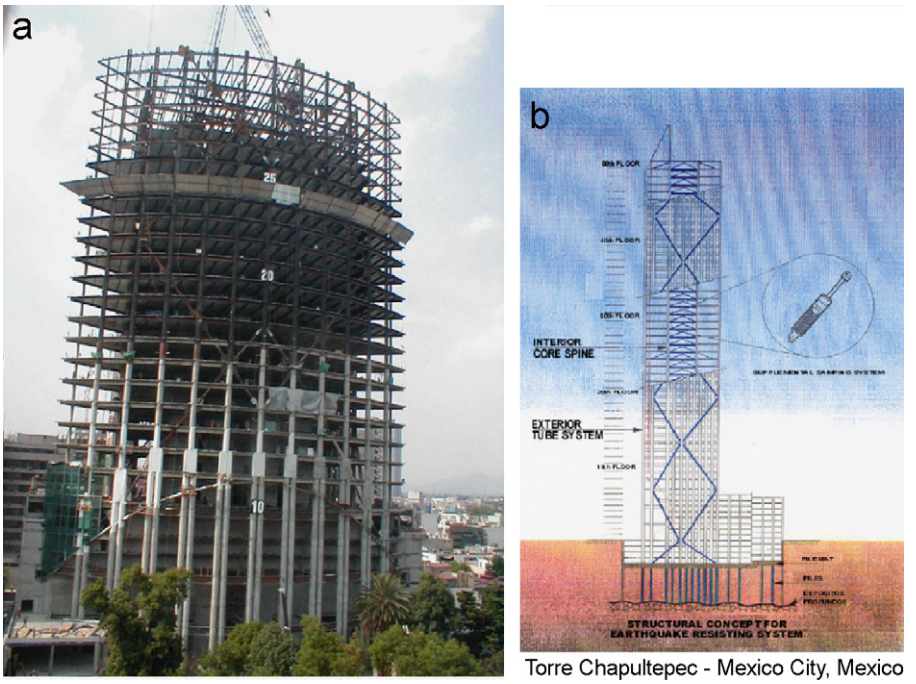

Fig. 13. The Chapultepec Tower (best known as Torre Major) in Mexico City: (a) under construction and (b) schematic representation of the "mega-braces" of Taylor Devices Company.

Fig. 14. (a) Osaka International Conference Centre, (b) Wallace F. Bennett Federal Building.

a "support" structure. This damper placement allows to obtain a dynamic system characterised by an exact MPD matrix, only if the "support" structure is infinitely stiff. Given that this is hardly physically feasible, the performances obtained by such systems cannot be the same of those obtained with the direct implementation of the MPD system. To address this issue, the authors have carried out an extensive parametric study varying the ratio between the lateral stiffness of the support and the reference structures. Given that the reference

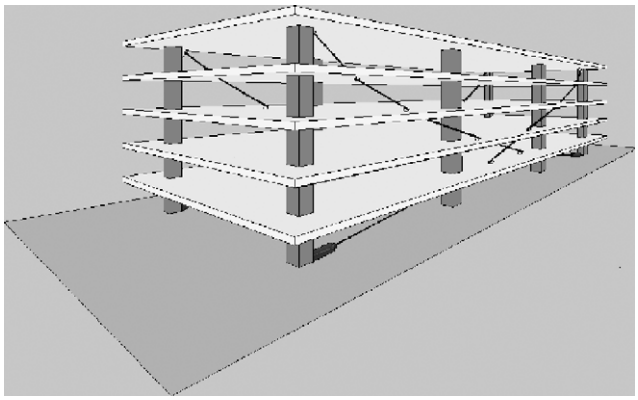

Fig. 15. Schematic representation of the damping cables of the SPIDER research project.

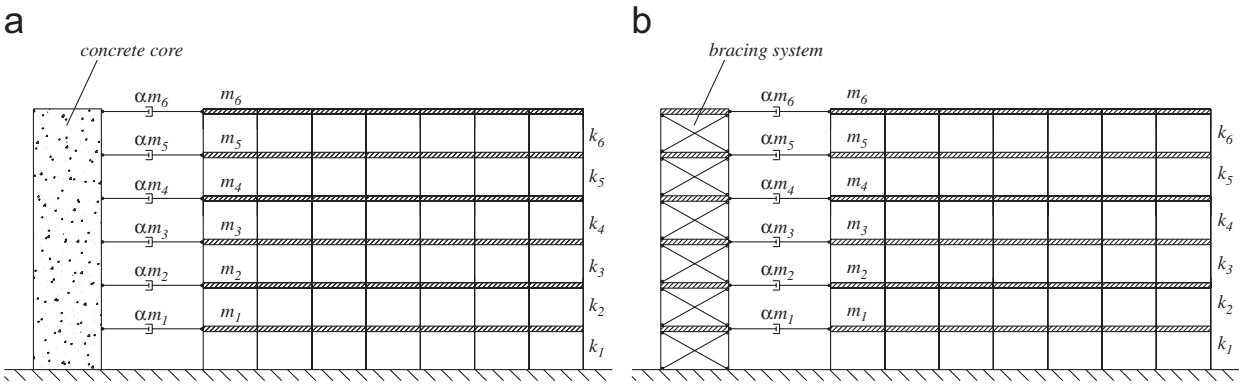

Fig. 16. MPD system obtained by placing dampers so that they connect the reference shear-type structure to (a) a concrete core and (b) a bracing system.

structure and the "support" structure can be either two adjacent buildings or two portions of the same building, this parametric study has been developed with reference to the following two cases:

- *Case* 1: insertion of dampers between two adjacent structures characterised by different dynamic properties;
- *Case* 2: insertion of dampers between a frame structure and a very stiff lateral-resisting element, such as the conventional concrete cores of the stairs/elevator typically found in r.c. constructions (Fig. 16a) or the bracing systems typical of steel structures (Fig. 16b).

It must be noticed that the coupling with viscous dampers of two structures has been investigated in recent research works [31–37] (even though not recognising it as an indirect implementation of the MPD system).

In the forthcoming Sections 7.1 and 7.2, the dynamic properties of the systems of cases 1 and 2 are studied individually.

7.1. Insertion of dampers between two adjacent structures characterised by different dynamic properties (case 1)

Let us consider the two structures represented in Fig. 17, where R denotes the reference structure and S denotes the support structure, both characterised by the same total number of storeys. The reference structure R considered in this illustrative example is the 6-storey shear-type structure described in Section 4

(characterised by floor masses $m_i = m$, $\forall i$ and storey lateral stiffnesses $k_i = k$, $\forall i$). Twelve different support structures S are considered in this parametric study, each one characterised by

- floor masses m_S equal to $m_S = \rho_m m$,
- storey lateral stiffnesses k_S equal to $k_S = \rho_k k$.

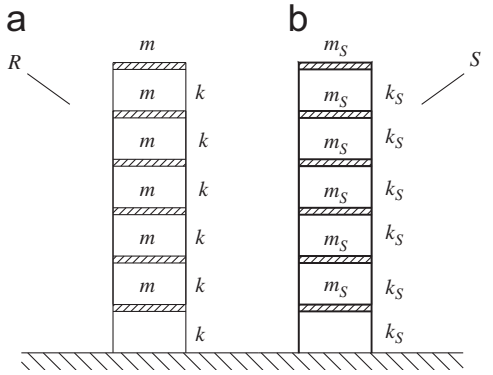

Fig. 17. (a) Reference structure R. (b) Support structure S.

Table 3
Values of ρ_m, ρ_k and $\rho_T = T_{1,S}/T_{1,R}$ for case 1

	ρ_m	ρ_k	ρ_T
S_1	0.75	2	0.612
S_2	0.75	5	0.387
S_3	0.75	10	0.274
S_4	0.75	20	0.194
S_5	1.00	2	0.707
S_6	1.00	5	0.447
S_7	1.00	10	0.316
S_8	1.00	20	0.224
S_9	1.50	2	0.866
S_{10}	1.50	5	0.548
S_{11}	1.50	10	0.387
S_{12}	1.50	20	0.274

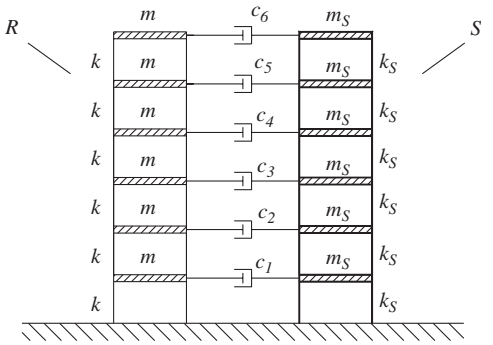

Fig. 18. Coupled structures R & S.

where ρ_m and ρ_k are given in Table 3. Table 3 also gives the ratio, ρ_T, between the fundamental period, $T_{1,S}$, of each support structure S and the fundamental period, $T_{1,R}$, of the reference structure R.

Note that the 12 support structures considered can be divided into three groups, each one characterised by the same ρ_m: S_1 through S_4 are characterised by $\rho_m = 0.75$, S_5 through S_8 are characterised by $\rho_m = 1.00$, and S_9 through S_{12} are characterised by $\rho_m = 1.50$.

The parametric study is carried out for the following dynamic systems (structures + equal "total size" ensemble of additional dampers):

- structure R with no added viscous dampers (and null internal damping), referred to as R-UND dynamic system, as per Fig. 17a;
- structure R equipped with the SPD system, referred to as R-SPD dynamic system, as per Fig. 7c and Table 2;

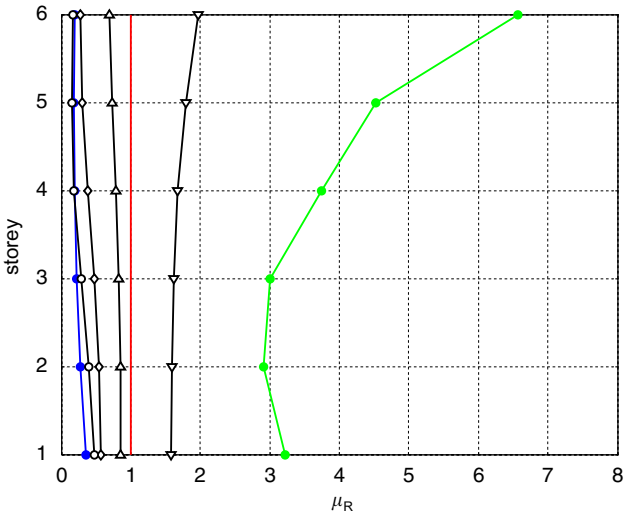

Fig. 19. Profiles of response ratio averages: (—▽—) $\mu_{\text{R-MPD-I}}$ for S_1, (—△—) $\mu_{\text{R-MPD-I}}$ for S_2, (—◇—) $\mu_{\text{R-MPD-I}}$ for S_3, (—○—) $\mu_{\text{R-MPD-I}}$ for S_4, (—●—, green) $\mu_{\text{R-UND}}$, and (—●—, blue) $\mu_{\text{R-MPD}}$, as computed for structure R.

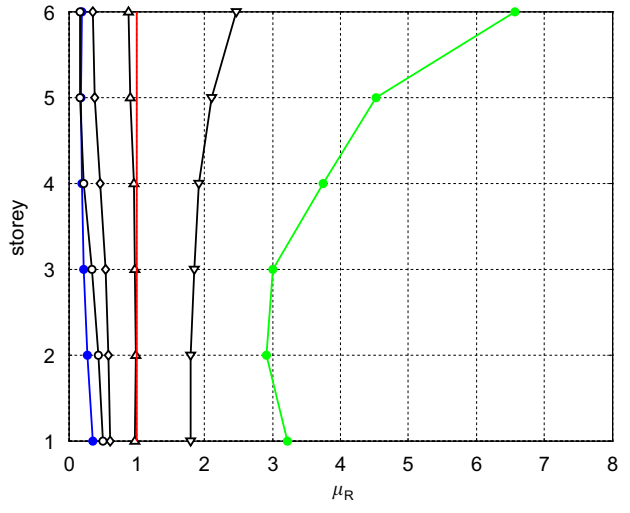

Fig. 20. Profiles of response ratio averages: (—▽—) $\mu_{\text{R-MPD-I}}$ for S_5, (—△—) $\mu_{\text{R-MPD-I}}$ for S_6, (—◇—) $\mu_{\text{R-MPD-I}}$ for S_7, (—○—) $\mu_{\text{R-MPD-I}}$ for S_8, (—●—, green) $\mu_{\text{R-UND}}$, and (—●—, blue) $\mu_{\text{R-MPD}}$, as computed for structure R.

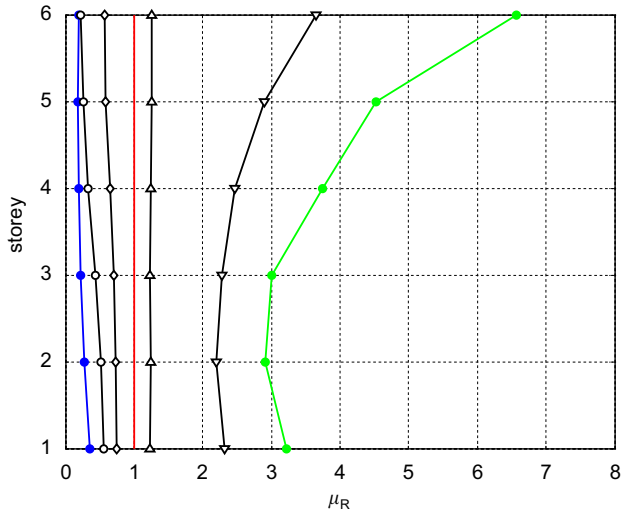

Fig. 21. Profiles of response ratio averages: (—▽—) $\mu_{\text{R-MPD-I}}$ for S_9, (—△—) $\mu_{\text{R-MPD-I}}$ for S_{10}, (—◇—) $\mu_{\text{R-MPD-I}}$ for S_{11}, (—○—) $\mu_{\text{R-MPD-I}}$ for S_{12}, (—●—, green) $\mu_{\text{R-UND}}$, and (—●—, blue) $\mu_{\text{R-MPD}}$, as computed for structure R.

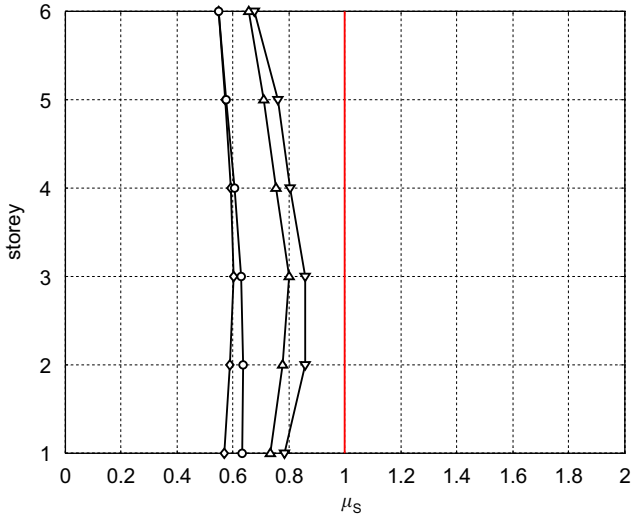

Fig. 22. Profiles of response ratio averages: (—▽—) $\mu_{\text{S-MPD-I}}$ for S_1, (—△—) $\mu_{\text{S-MPD-I}}$ for S_2, (—◇—) $\mu_{\text{S-MPD-I}}$ for S_3, (—○—) $\mu_{\text{S-MPD-I}}$ for S_4, as computed for structure S.

- structure R equipped with the MPD system (direct implementation), referred to as R-MPD dynamic system, as per Fig. 7b and Table 2;
- structure S with no added viscous dampers (and null internal damping), referred to as S-UND dynamic system, as per Fig. 17b;
- indirect implementation of the MPD system. The indirect implementation is obtained placing the same dampers of the R-MPD dynamic system between the corresponding storey of structure R and structure S, as per Fig. 18 and Table 2. This dynamic system will be referred to as RS-MPD-I dynamic system. The response of structure R is referred to as the response of R-MPD-I dynamic system and the response of structure S is referred to as the response of S-MPD-I dynamic system.

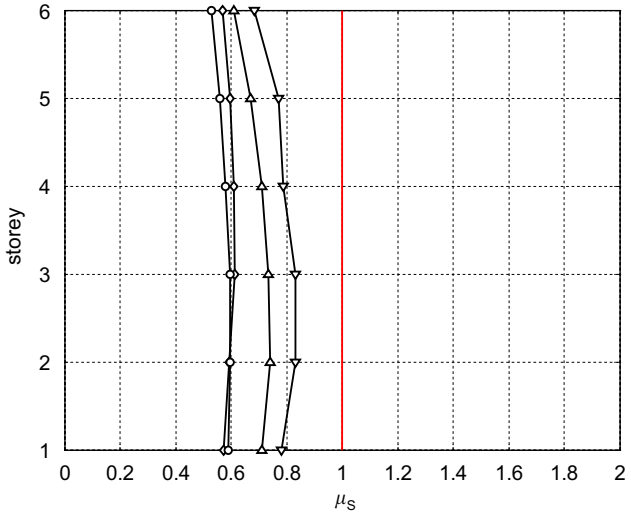

Fig. 23. Profiles of response ratio averages: (—▽—) $\mu_{\text{S-MPD-I}}$ for S_5, (—△—) $\mu_{\text{S-MPD-I}}$ for S_6, (—◇—) $\mu_{\text{S-MPD-I}}$ for S_7, (—○—) $\mu_{\text{S-MPD-I}}$ for S_8, as computed for structure S.

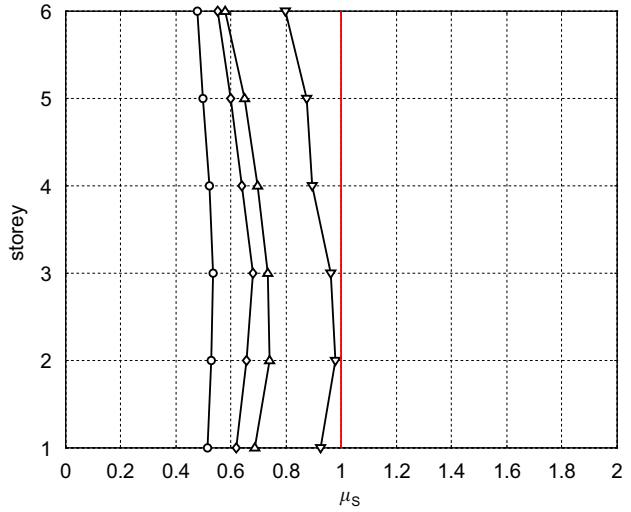

Fig. 24. Profiles of response ratio averages: (—▽—) $\mu_{\text{S-MPD-I}}$ for S_9, (—△—) $\mu_{\text{S-MPD-I}}$ for S_{10}, (—◇—) $\mu_{\text{S-MPD-I}}$ for S_{11}, (—○—) $\mu_{\text{S-MPD-I}}$ for S_{12}, as computed for structure S.

Note that, due to the equal "total size" constraint and the properties of the structure, each damper of the ensemble of 6 dampers inserted in the R-SPD, R-MPD and RS-MPD-I dynamic systems is characterised by a damping coefficient c_j equal to $\bar{c}/6 = 1.5 \times 10^6$ N × s/m.

The response of the above dynamic systems is numerically computed under the effects of 40 historically recorded earthquake ground motions. Out of these, 30 are far-field records and 10 near-field records; all records are scaled to the same PGA value of $0.3g$.

For structure R, for each earthquake, taking as reference the maximum shear developed by the R-SPD dynamic system at each ith storey, the following storey response ratios can be computed:

$$(r_i)_{\text{R-UND}} = \frac{(V_{\max -i})_{\text{R-UND}}}{(V_{\max -i})_{\text{R-SPD}}}, \tag{32}$$

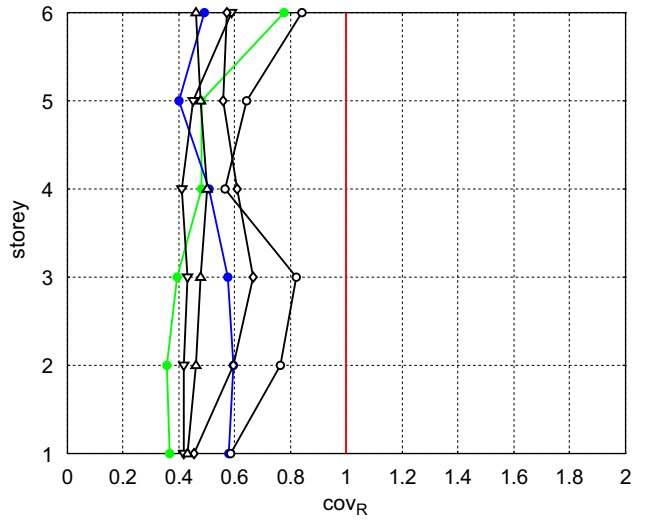

Fig. 25. Profiles of the coefficient of variation of the response ratio averages: (—▽—) $\mathrm{cov}_{\text{R-MPD-I}}$ for S_1, (—△—) $\mathrm{cov}_{\text{R-MPD-I}}$ for S_2, (—◇—) $\mathrm{cov}_{\text{R-MPD-I}}$ for S_3, (—○—) $\mathrm{cov}_{\text{R-MPD-I}}$ for S_4, (—●—, green) $\mathrm{cov}_{\text{R-UND}}$, and (—●—, blue) $\mathrm{cov}_{\text{R-MPD}}$, as computed for structure R.

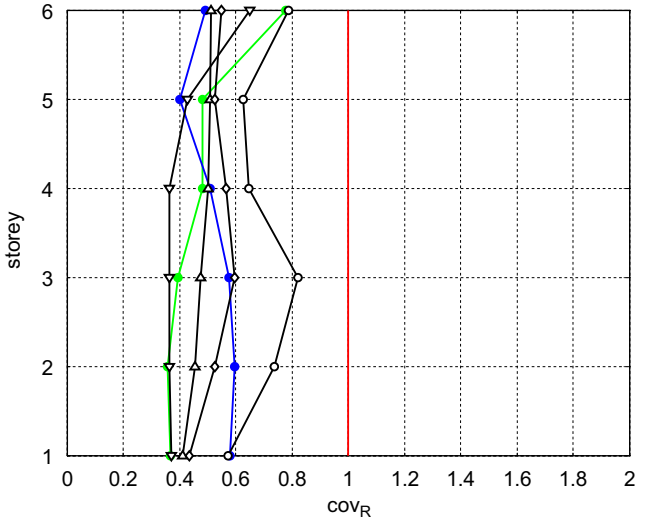

Fig. 26. Profiles of the coefficient of variation of the response ratio averages: (—▽—) $\mathrm{cov}_{\text{R-MPD-I}}$ for S_5, (—△—) $\mathrm{cov}_{\text{R-MPD-I}}$ for S_6, (—◇—) $\mathrm{cov}_{\text{R-MPD-I}}$ for S_7, (—○—) $\mathrm{cov}_{\text{R-MPD-I}}$ for S_8, (—●—, green) $\mathrm{cov}_{\text{R-UND}}$, and (—●—, blue) $\mathrm{cov}_{\text{R-MPD}}$, as computed for structure R.

$$(r_i)_{\text{R-MPD}} = \frac{(V_{\max -i})_{\text{R-MPD}}}{(V_{\max -i})_{\text{R-SPD}}}, \tag{33}$$

$$(r_i)_{\text{R-MPD-I}} = \frac{(V_{\max -i})_{\text{R-MPD-I}}}{(V_{\max -i})_{\text{R-SPD}}}, \tag{34}$$

where $(V_{\max -i})_{\text{R-UND}}$, $(V_{\max -i})_{\text{R-SPD}}$, $(V_{\max -i})_{\text{R-MPD}}$ and $(V_{\max -i})_{\text{R-MPD-I}}$ denote the maximum shear at the ith storey developed, respectively, by the R-UND, R-SPD, R-MPD and R-MPD-I dynamic systems.

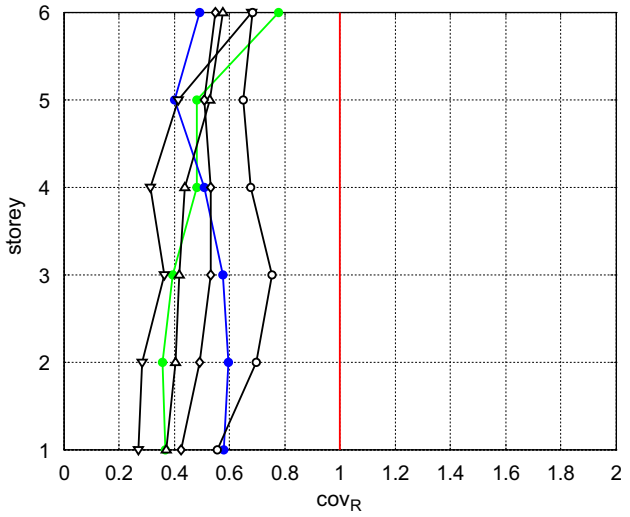

Fig. 27. Profiles of the coefficient of variation of the response ratio averages: (—▽—) $\mathrm{cov}_{\text{R-MPD-I}}$ for S_9, (—△—) $\mathrm{cov}_{\text{R-MPD-I}}$ for S_{10}, (—◇—) $\mathrm{cov}_{\text{R-MPD-I}}$ for S_{11}, (—○—) $\mathrm{cov}_{\text{R-MPD-I}}$ for S_{12}, (—●—, green) $\mathrm{cov}_{\text{R-UND}}$, and (—●—, blue) $\mathrm{cov}_{\text{R-MPD}}$, as computed for structure R.

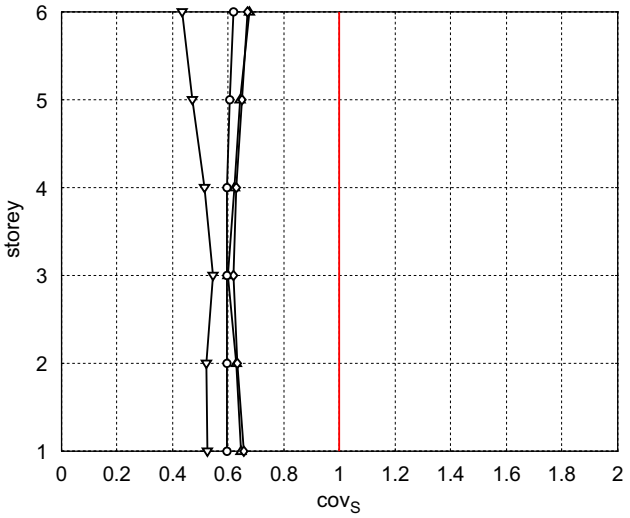

Fig. 28. Profiles of the coefficient of variation of the response ratio averages: (—▽—) $\mathrm{cov}_{\text{S-MPD-I}}$ for S_1, (—△—) $\mathrm{cov}_{\text{S-MPD-I}}$ for S_2, (—◇—) $\mathrm{cov}_{\text{S-MPD-I}}$ for S_3 and (—○—) $\mathrm{cov}_{\text{S-MPD-I}}$ for S_4, as computed for structure S.

For structure S, for each earthquake, taking as reference the maximum shear developed by the S-UND dynamic system at each ith storey, the following storey response ratio can be computed:

$$(r_i)_{\text{S-MPD-I}} = \frac{(V_{\max -i})_{\text{S-MPD-I}}}{(V_{\max -i})_{\text{S-UND}}}, \tag{35}$$

where $(V_{\max -i})_{\text{S-UND}}$ and $(V_{\max -i})_{\text{S-MPD-I}}$ denote the maximum shear at the ith storey developed, respectively, by the S-UND and S-MPD-I dynamic systems.

The means of the response ratios given by Eqs. (32)–(35), for all 40 earthquakes considered, are referred to, respectively, as $\mu_{\text{R-UND}}$, $\mu_{\text{R-MPD}}$, $\mu_{\text{R-MPD-I}}$ and $\mu_{\text{S-MPD-I}}$. The coefficients of variations of the response ratios given by Eqs. (32)–(35), for all 40 earthquakes considered, are referred to, respectively, as $\mathrm{cov}_{\text{R-UND}}$,

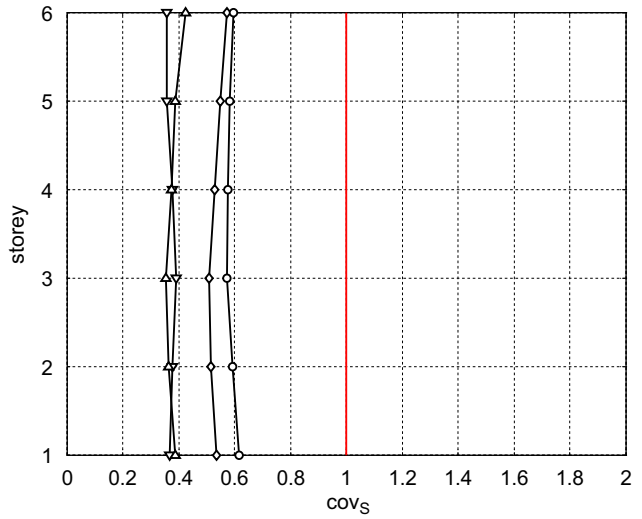

Fig. 29. Profiles of the coefficient of variation of the response ratio averages: (—▽—) $\mathrm{cov}_{\text{S-MPD-I}}$ for S_5, (—△—) $\mathrm{cov}_{\text{S-MPD-I}}$ for S_6, (—◇—) $\mathrm{cov}_{\text{S-MPD-I}}$ for S_7 and (—○—) $\mathrm{cov}_{\text{S-MPD-I}}$ for S_8, as computed for structure S.

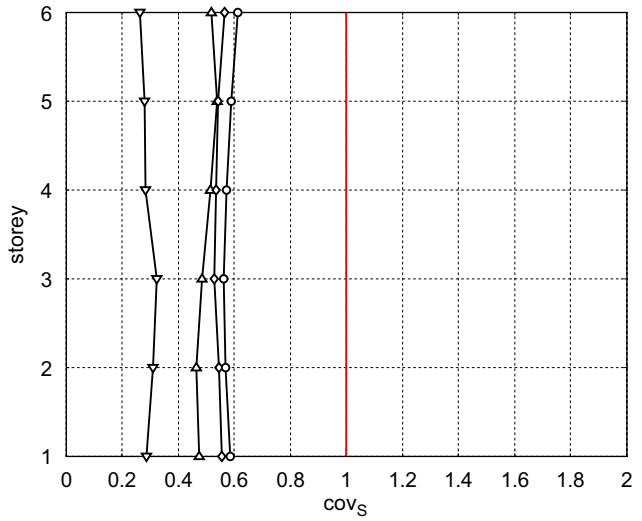

Fig. 30. Profiles of the coefficient of variation of the response ratio averages: (—▽—) $\mathrm{cov}_{\text{S-MPD-I}}$ for S_9, (—△—) $\mathrm{cov}_{\text{S-MPD-I}}$ for S_{10}, (—◇—) $\mathrm{cov}_{\text{S-MPD-I}}$ for S_{11} and (—○—) $\mathrm{cov}_{\text{S-MPD-I}}$ for S_{12}, as computed for structure S.

$\mathrm{cov}_{\text{R-MPD}}$, $\mathrm{cov}_{\text{R-MPD-I}}$ and $\mathrm{cov}_{\text{S-MPD-I}}$. In general, μ_R and cov_R will be, respectively, used to indicate the means and the coefficients of variation of a generic response ratio given by Eqs. (32)–(34).

The plots of $\mu_{\text{R-MPD-I}}$ as obtained for the case of structures S_1, S_2, S_3 and S_4 used as support structures in the RS-MPD-I dynamic system (all characterised by $\rho_m = 0.75$) are represented in Fig. 19, which also plots $\mu_{\text{R-UND}}$ and $\mu_{\text{R-MPD}}$ as reference values. Inspection of Fig. 19 indicates that, for the dynamic system composed of the reference structure R and the support structure S_1 (characterised by $\rho_k = 2$), the indirect implementation of the MPD system leads to a response ratio average μ_R which is smaller (−50% to −70%) than that of the R-UND dynamic system, but still larger (+60% to +100%) than that of the R-SPD dynamic system. On the other hand, for the dynamic systems composed of the reference structure R and the support structures S_2, S_3 and S_4 (characterised, respectively, by $\rho_k = 5$, 10 and 20), the indirect implementation of the MPD system leads to a response ratio average μ_R which is smaller than that of the R-SPD dynamic system. Note that for the dynamic system which uses S_4 as support structure, $\mu_{\text{R-MPD-I}}$ is

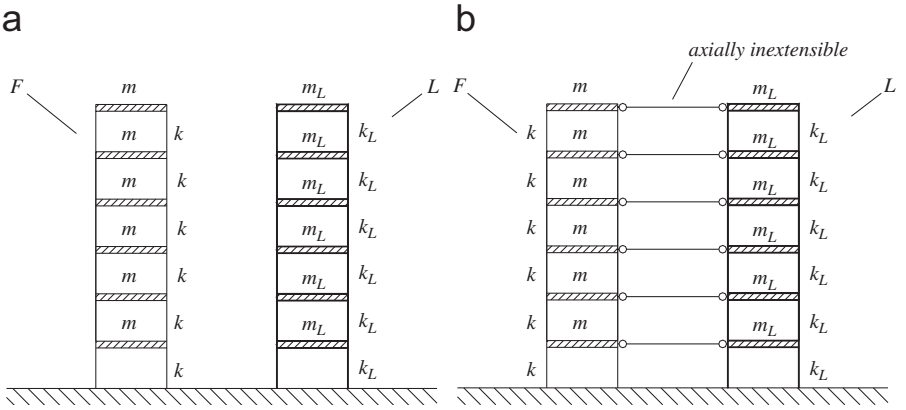

Fig. 31. (a) Frame structure F and lateral-resisting element L. (b) FL structural system.

Table 4
Values of ρ_m, ρ_k and $\rho_T = T_{1,L}/T_{1,F}$ for case 2

	ρ_m	ρ_k	ρ_T
L_1	0.02	5	0.063
L_2	0.02	10	0.045
L_3	0.02	20	0.032
L_4	0.02	50	0.020
L_5	0.05	5	0.100
L_6	0.05	10	0.071
L_7	0.05	20	0.050
L_8	0.05	50	0.032
L_9	0.10	5	0.141
L_{10}	0.10	10	0.100
L_{11}	0.10	20	0.071
L_{12}	0.10	50	0.045

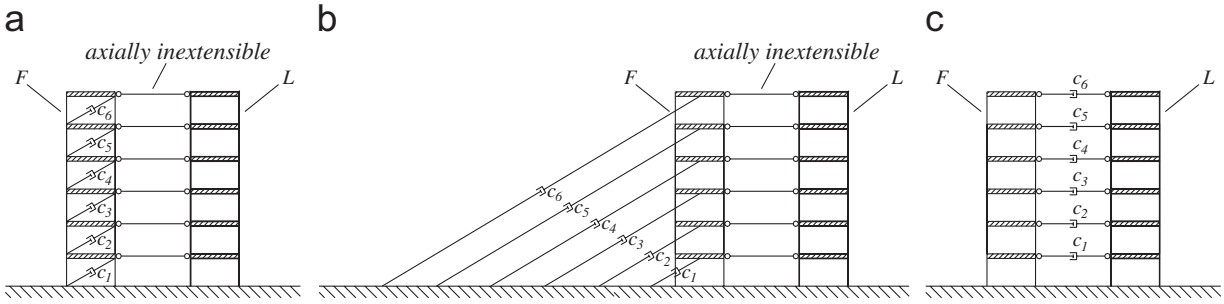

Fig. 32. (a) FL-SPD dynamic system. (b) FL-MPD dynamic system. (c) FL-MPD-I dynamic system.

comparable to $\mu_{\text{R-MPD}}$. In summary, these results indicate that, for systems characterised by $\rho_m = 0.75$, the indirect implementation of the MPD system:

- allows to obtain a seismic response of the reference structure R which is smaller than that of the same structure equipped with the SPD system, for structures characterised by a stiffness ratio ρ_k larger than 5;
- allows to obtain a seismic response of the reference structure R which is similar to that of the same structure equipped with the MPD system, for structures characterised by a stiffness ratio ρ_k larger than 20.

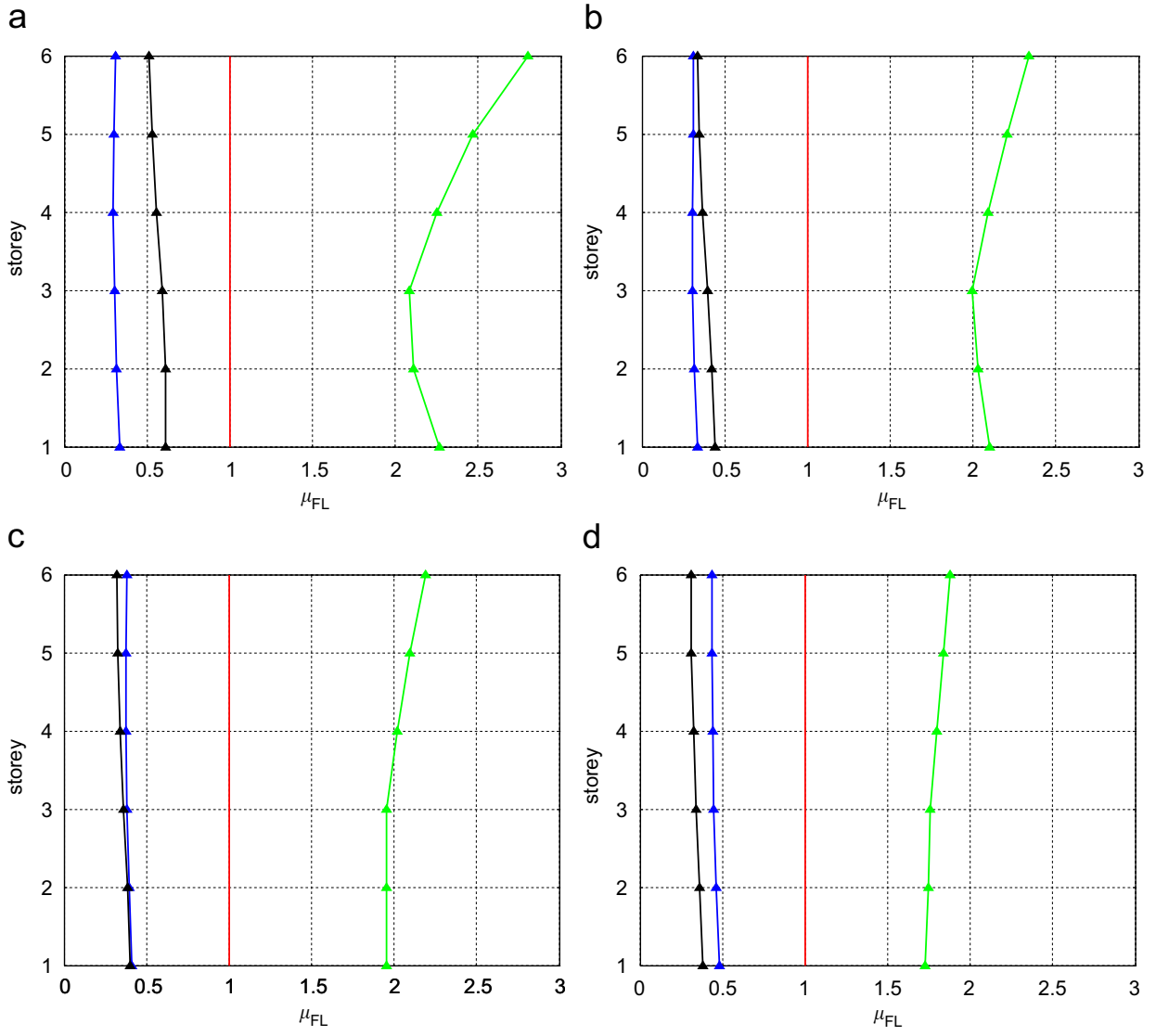

Fig. 33. Profiles of response ratio averages (green) $\mu_{\text{FL-UND}}$, (blue) $\mu_{\text{FL-MPD}}$ and (black) $\mu_{\text{FL-MPD-I}}$: (a) L_1, (b) L_2, (c) L_3 and (d) L_4.

The plots of $\mu_{\text{R-MPD-I}}$, as obtained for the case of structures S_5, S_6, S_7 and S_8 used as support structures in the RS-MPD-I dynamic system (all characterised by $\rho_m = 1.00$), $\mu_{\text{R-UND}}$ and $\mu_{\text{R-MPD}}$ are not reported here for sake of conciseness but are available in the online version of this article as Electronic Fig. 20. Inspection of these plots indicates that, for the dynamic system composed of the reference structure R and the support structure S_5 (characterised by $\rho_k = 2$), the indirect implementation of the MPD system leads to a response ratio average μ_R which is smaller (-35% to -65%) than that of the R-UND dynamic system, but substantially larger ($+80\%$ to $+150\%$) than that of the R-SPD dynamic system. For the dynamic system composed of the reference structure R and the support structure S_6 (characterised by $\rho_k = 5$), the indirect implementation of the MPD system leads to a response ratio average μ_R which is similar to that of the R-SPD dynamic system. On the other hand, for the dynamic systems composed of the reference structure R and the support structures S_7 and S_8 (characterised, respectively, by $\rho_k = 10$ and 20), the indirect implementation of MPD system leads to a response ratio average μ_R which is smaller than that of the R-SPD dynamic system. Note that, as in the above previous case, for the dynamic system which uses S_8 as support structure, $\mu_{\text{R-MPD-I}}$

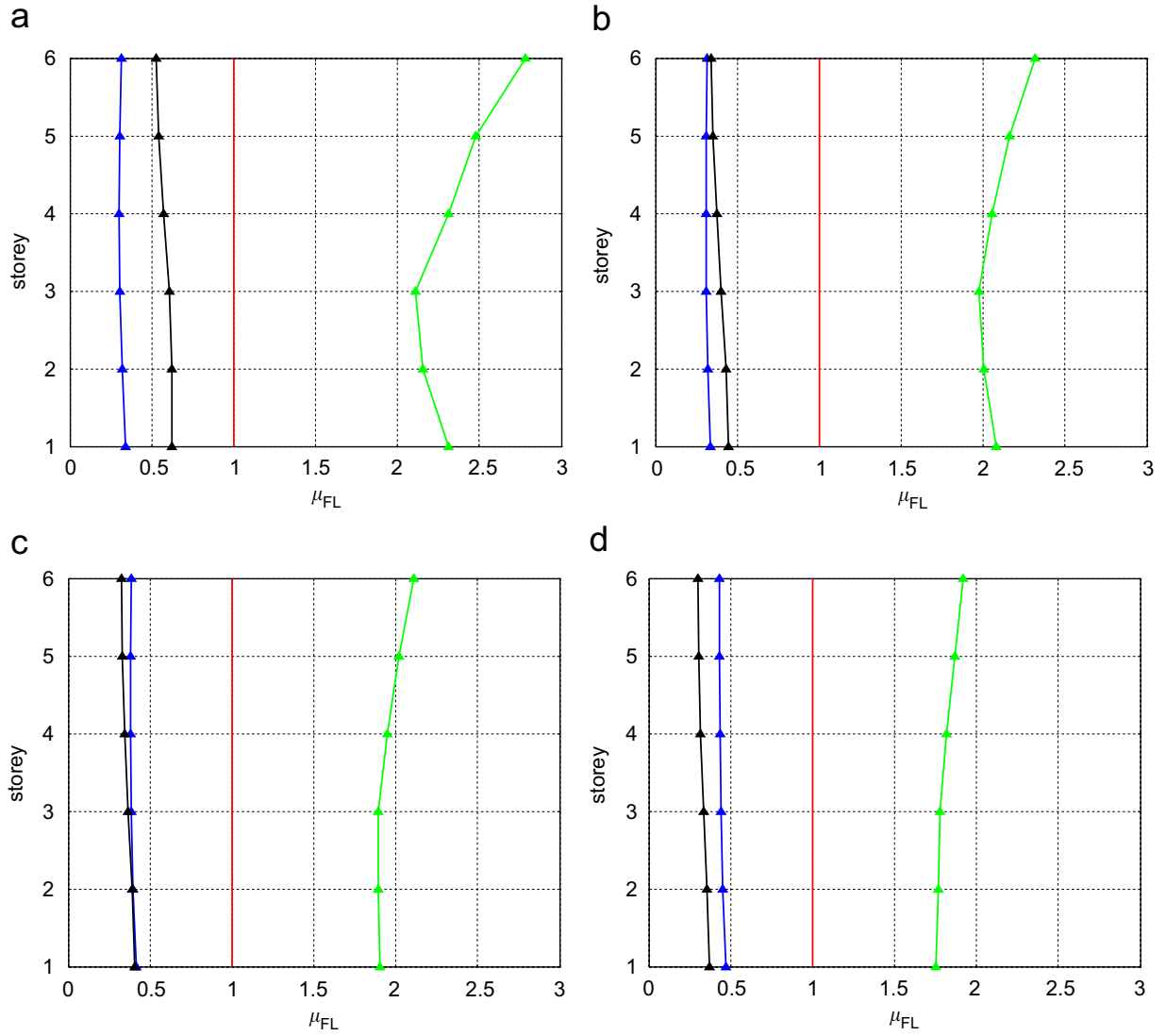

Fig. 34. Profiles of response ratio averages (green) $\mu_{\text{FL-UND}}$, (blue) $\mu_{\text{FL-MPD}}$ and (black) $\mu_{\text{FL-MPD-I}}$: (a) L_5, (b) L_6, (c) L_7 and (d) L_8.

is comparable to $\mu_{\text{R-MPD}}$. In summary, these results indicate that, for systems characterised by $\rho_m = 1.00$, the indirect implementation of the MPD system:

- allows to obtain a seismic response of the reference structure R which is smaller than that of the same structure equipped with the SPD system, for structures characterised by a stiffness ratio ρ_k larger than 10;
- allows to obtain a seismic response of the reference structure R which is similar to that of the same structure equipped with the MPD system, for structures characterised by a stiffness ratio ρ_k larger than 20.

The plots of $\mu_{\text{R-MPD-I}}$, as obtained for the case of structures S_9, S_{10}, S_{11} and S_{12} used as support structures in the RS-MPD-I dynamic system (all characterised by $\rho_m = 1.50$), $\mu_{\text{R-UND}}$ and $\mu_{\text{R-MPD}}$ are not reported here for sake of conciseness but are available in the online version of this article as Electronic Fig. 21. Inspection of these plots indicates that the dynamic systems composed of the reference structure R and the support structures S_9 and S_{10} (characterised, respectively, by $\rho_k = 2$ and 5), the indirect implementation of the MPD system leads to a response ratio average μ_R which is smaller than that of the R-UND dynamic system, but

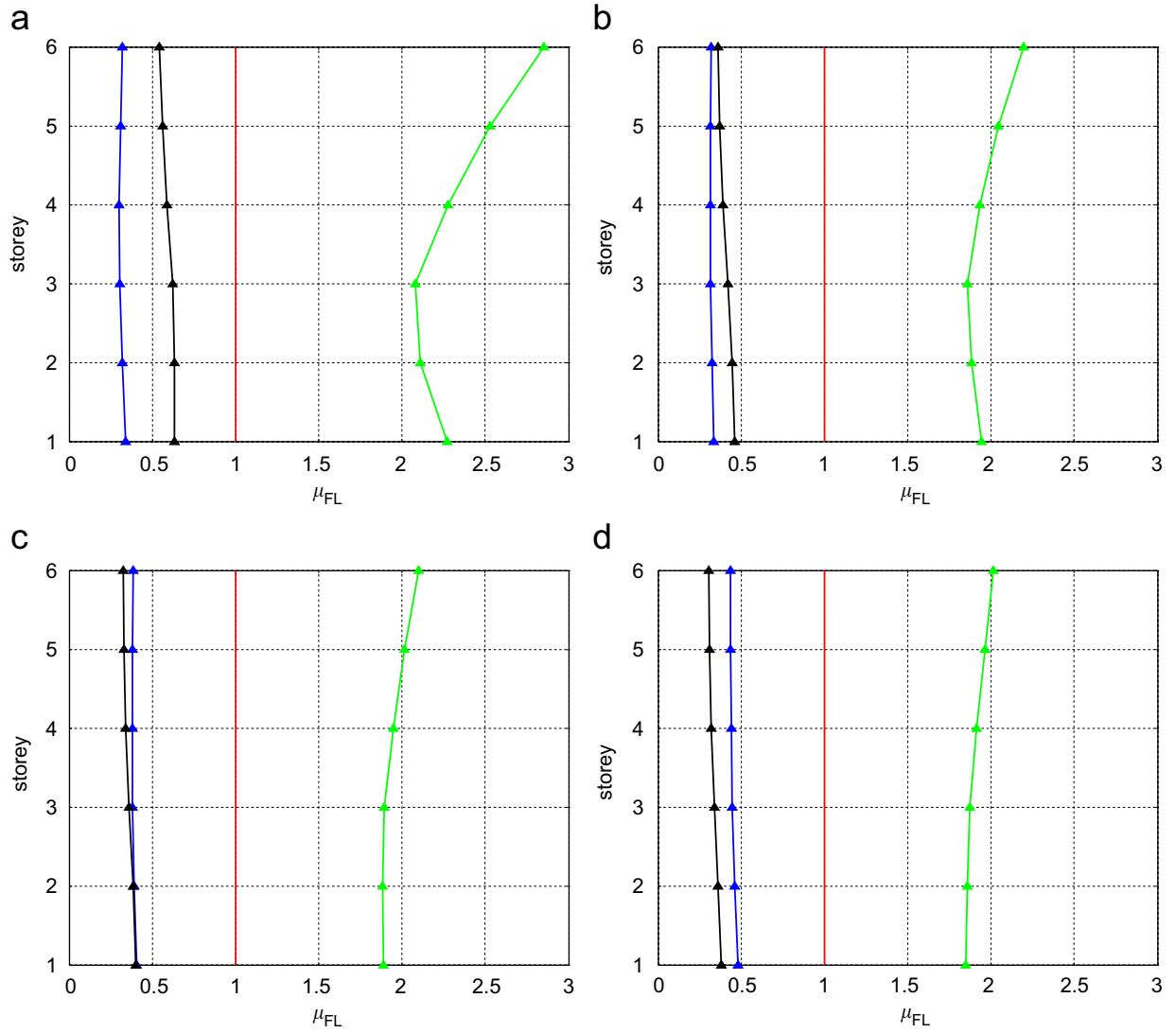

Fig. 35. Profiles of response ratio averages (green) $\mu_{\text{FL-UND}}$, (blue) $\mu_{\text{FL-MPD}}$ and (black) $\mu_{\text{FL-MPD-I}}$: (a) L_9, (b) L_{10}, (c) L_{11} and (d) L_{12}.

substantially larger than that of the R-SPD dynamic system. On the other hand, for the dynamic systems composed of the reference structure R and the support structures S_{11} and S_{12} (characterised, respectively, by $\rho_k = 10$ and 20), the indirect implementation of the MPD system leads to a response ratio average μ_R which is smaller than that of the R-SPD dynamic system. Also in this case, for the dynamic system which uses S_{12} as support structure, $\mu_{\text{R-MPD-I}}$ is comparable to $\mu_{\text{R-MPD}}$. In summary, these results indicate that, for systems characterised by $\rho_m = 1.50$, the indirect implementation of the MPD system:

- allows to obtain a seismic response of the reference structure R which is smaller than that of the same structure equipped with the SPD system, for structures characterised by a stiffness ratio ρ_k larger than 10;
- allows to obtain a seismic response of the reference structure R which is similar to that of the same structure equipped with the MPD system, for structures characterised by a stiffness ratio ρ_k larger than 20.

Inspection of Figs. 19–21 indicate that, in all three cases considered ($\rho_m = 0.75$, 1.00 and 1.50), when ρ_m is kept constant, with the increase of ρ_k, the vibration reduction effect gets better and better. This could be reasonably expected given that:

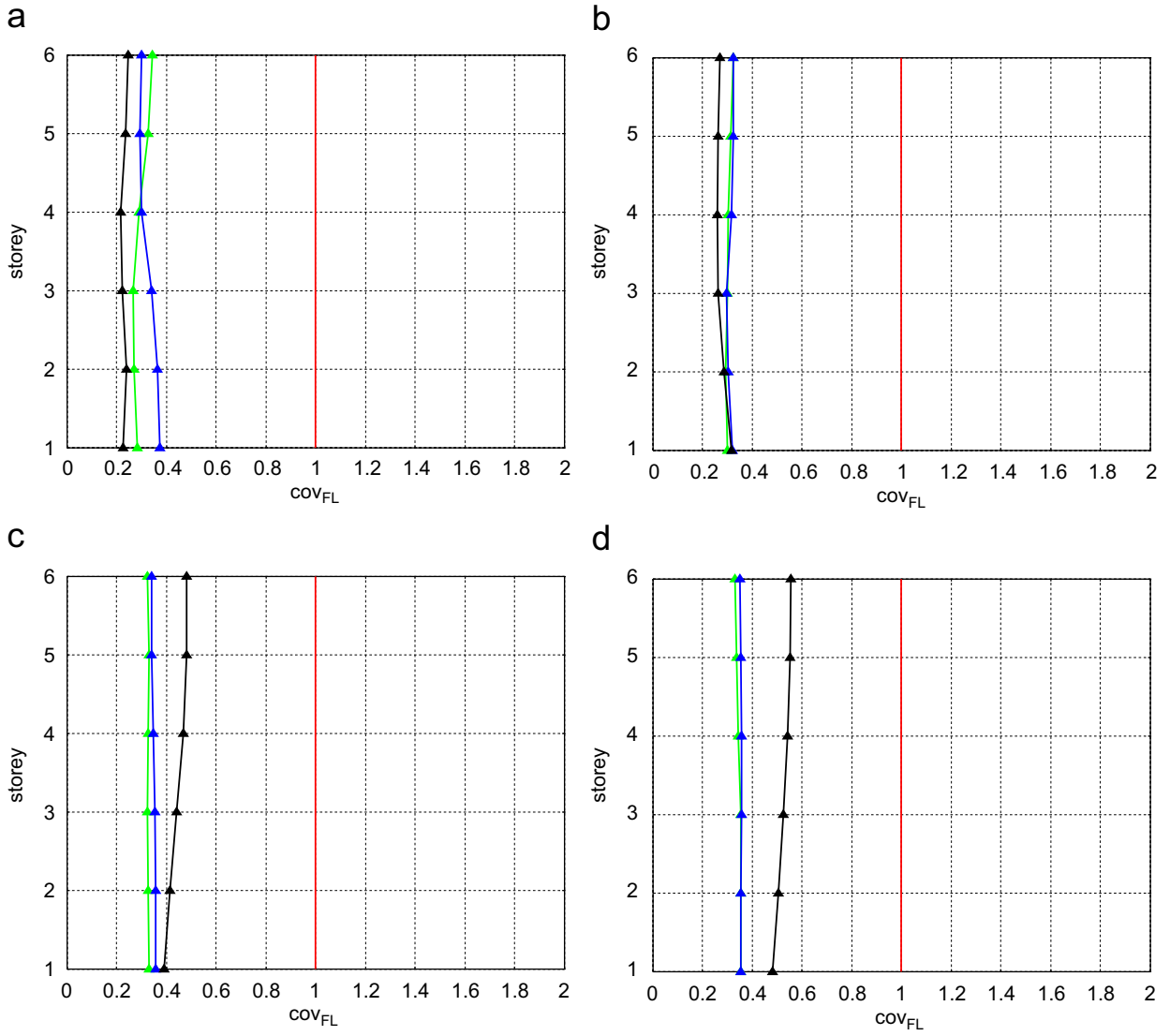

Fig. 36. Profiles of the coefficient of variation of the response ratios (green) $cov_{FL\text{-}UND}$, (blue) $cov_{FL\text{-}MPD}$ and (black) $cov_{FL\text{-}MPD\text{-}I}$: (a) L_1, (b) L_2, (c) L_3 and (d) L_4.

- when ρ_k tends to zero, the structure R of Fig. 18 tends to an undamped dynamic system;
- when ρ_k tends to infinity, the structure R of Fig. 18 tends to a dynamic system characterised by an exact MPD matrix (MPD system obtained with the FP-placement represented in Fig. 12e);
- systems characterised by an exact MPD matrix, as recalled in Section 4, provide higher dissipative efficiency than systems characterised by an SPD matrix.

Fig. 22 plots for each storey $\mu_{S\text{-}MPD\text{-}I}$ as obtained for the case of structures S_1, S_2, S_3 and S_4 used as support structures in the RS-MPD-I dynamic system. Fig. 23 (not reported here but available in the online version of this article) plots for each storey $\mu_{S\text{-}MPD\text{-}I}$ as obtained for the case of structures S_5, S_6, S_7 and S_8 used as support structures in the RS-MPD-I dynamic system. Fig. 24 (not reported here but available in the online version of this article) plots for each storey $\mu_{S\text{-}MPD\text{-}I}$ as obtained for the case of structures S_9, S_{10}, S_{11} and S_{12} used as support structures in the RS-MPD-I dynamic system.

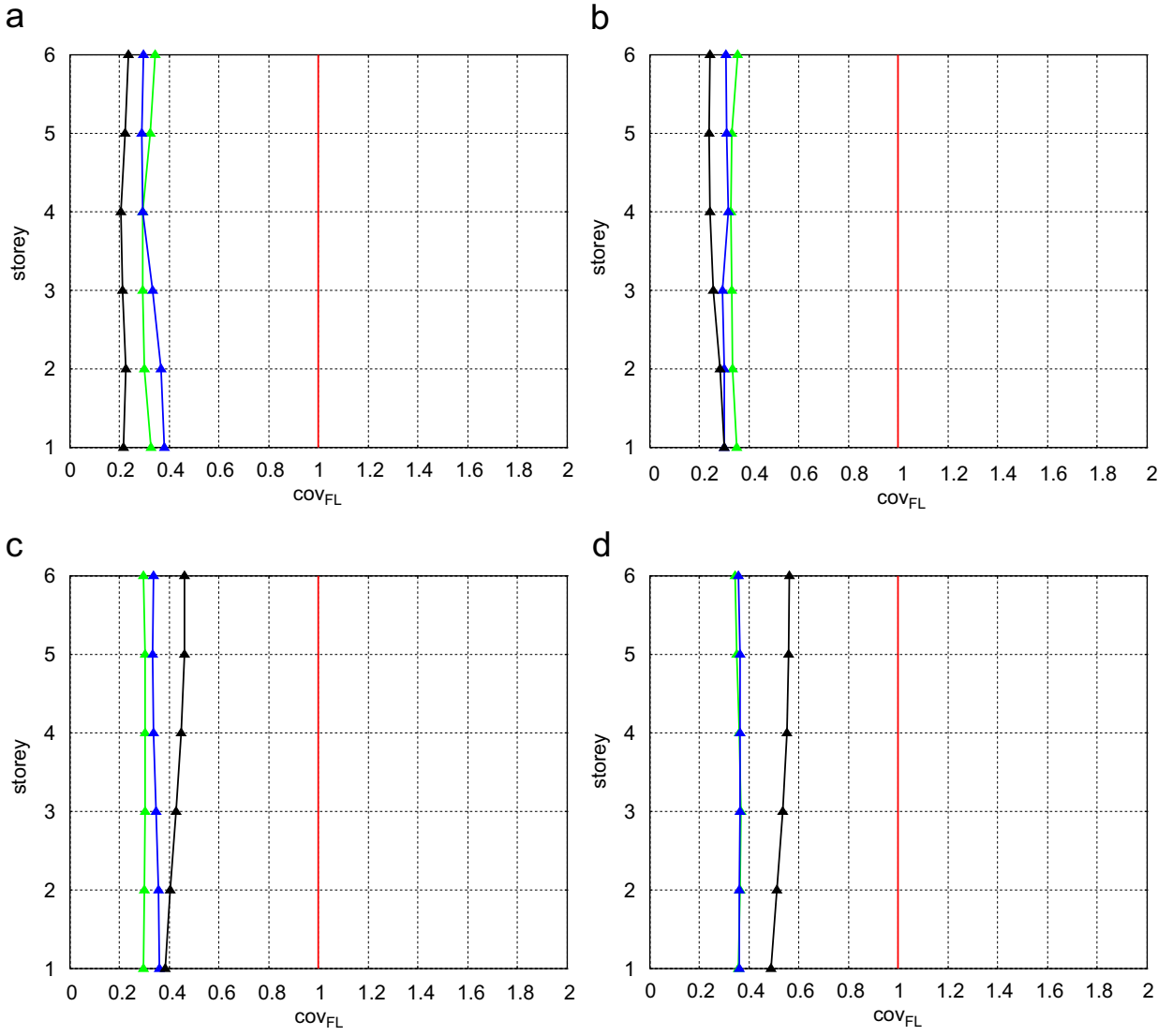

Fig. 37. Profiles of the coefficient of variation of the response ratios (green) $cov_{FL\text{-}UND}$, (blue) $cov_{FL\text{-}MPD}$ and (black) $cov_{FL\text{-}MPD\text{-}I}$: (a) L_5, (b) L_6, (c) L_7 and (d) L_8.

Inspection of Figs. 22–24 indicates that, for all dynamic systems considered, the indirect implementation of the MPD system leads to response ratio averages $\mu_{S\text{-}MPD\text{-}I}$ which are smaller than unity. This means that, as far as the support structure S is concerned, the indirect implementation of the MPD system leads to an improvement of its seismic response (with respect to that of the S-UND dynamic system).

The coefficients of variation of the response ratios for both R and S structures result to be within the range 0.4–0.8, as illustrated in Figs. 25–30 (Figs. 26, 27, 29 and 30 are not reported here but are available in the online version of this article).

To sum up, taking into account both the results obtained for the mean and the coefficients of variations of the response ratios, it can be deduced that, for adjacent structures characterised by similar masses (ρ_m in the range of 0.75–1.50):

- in order to obtain a reduction of the seismic response of the reference structure through the indirect implementation of the MPD system which is superior to that obtainable through the implementation of the

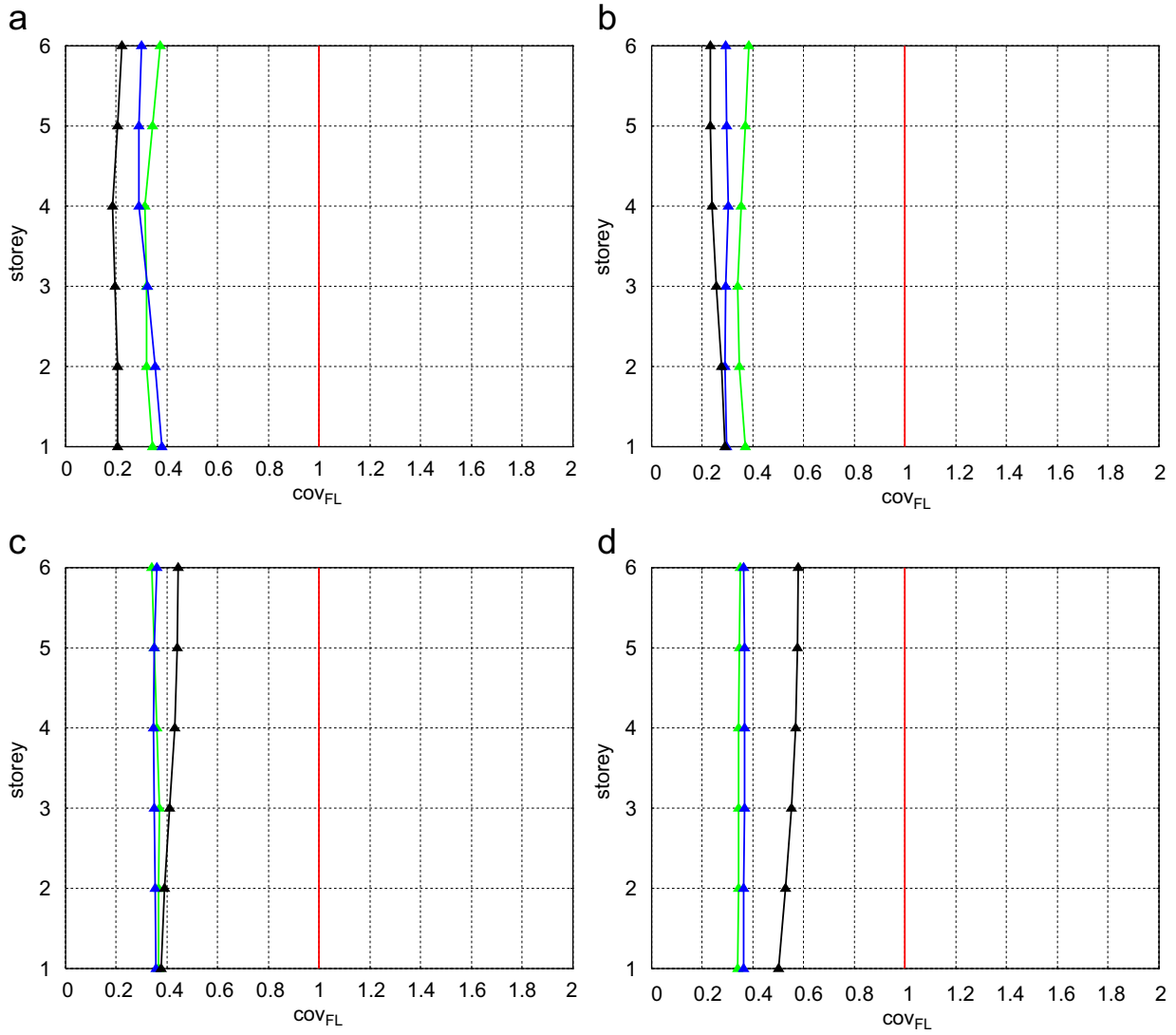

Fig. 38. Profiles of the coefficient of variation of the response ratios (green) $cov_{FL\text{-}UND}$, (blue) $cov_{FL\text{-}MPD}$ and (black) $cov_{FL\text{-}MPD\text{-}I}$: (a) L_9, (b) L_{10}, (c) L_{11} and (d) L_{12}.

equal "total size" SPD system, it is necessary that the support structure be characterised by lateral stiffness which is, at least, roughly 10 times larger than that of the reference structure (which may prove to be an unlikely condition);

- the support structures benefit in most cases by the introduction of an indirect MPD system.

7.2. *Insertion of dampers between a frame structure and a very stiff lateral-resisting element (case 2)*

Let us now consider the frame structure (denoted as F) and the lateral-resisting element (denoted as L) represented in Fig. 31a, both characterised by the same total number of storeys. By rigidly connecting F and L at each storey leads to the structural system represented in Fig. 31b (denoted as FL structural system). The FL structural system is representative of the common structural system in which a frame structure characterised by a relatively small lateral stiffness (typically nonmoment-resisting frame) is laterally supported by a very stiff

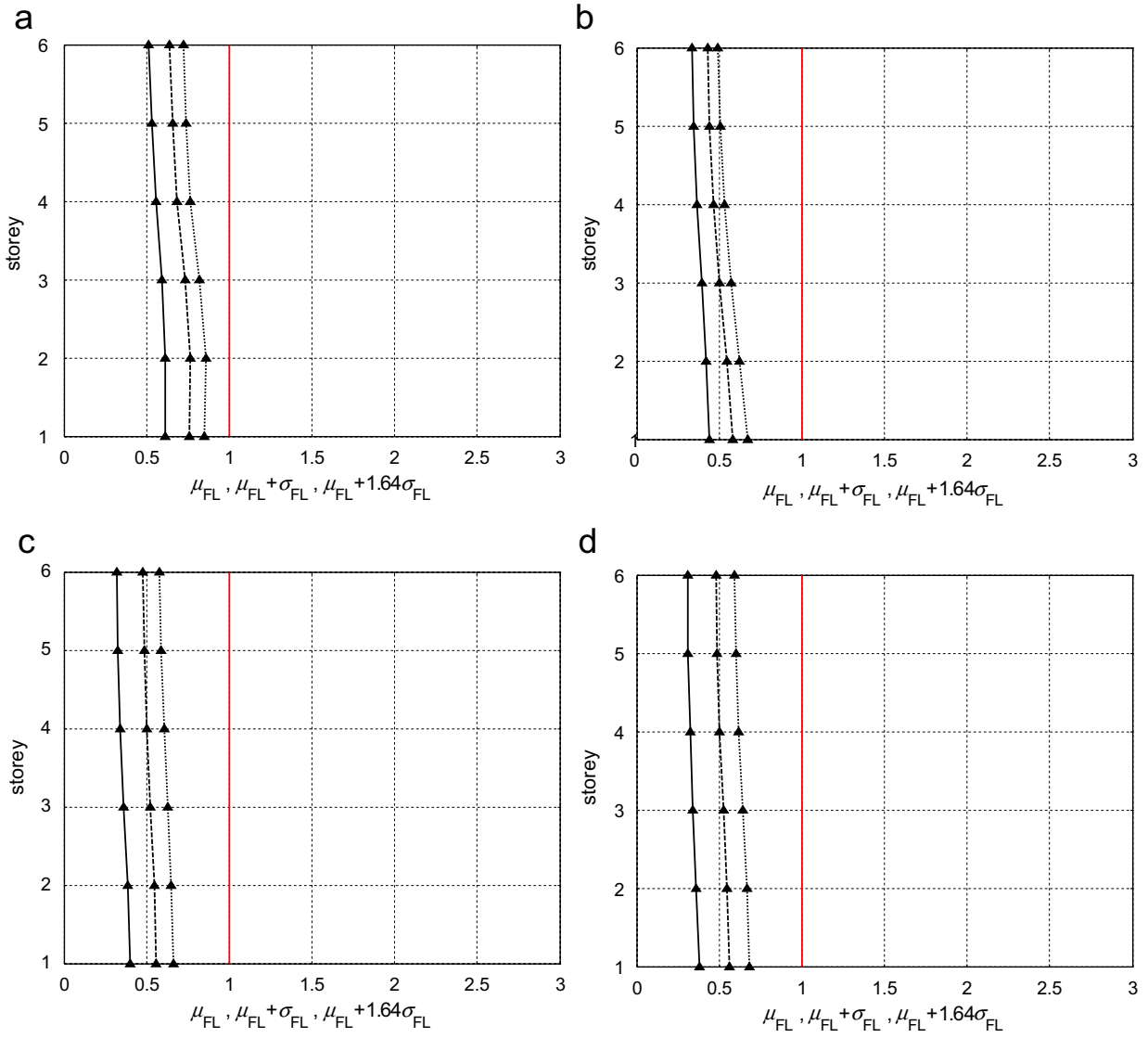

Fig. 39. Profiles of $\mu_{\text{FL-MPD-I}}$ (black continuous line), $\mu_{\text{FL-MPD-I}}+\sigma_{\text{FL-MPD-I}}$ (black dashed line) and $\mu_{\text{FL-MPD-I}}+1.64\sigma_{\text{FL-MPD-I}}$ (black dotted line): (a) L_1, (b) L_2, (c) L_3 and (d) L_4.

lateral-resisting element (such as shear wall, concrete core, bracing system, etc.). The frame structure F considered in this illustrative example is the 6-storey shear-type structure described in Section 4 (characterised by floor masses $m_i = m$, $\forall i$, and storey lateral stiffnesses $k_i = k$, $\forall i$). Twelve different lateral-resisting elements L are considered in this illustrative example, each one characterised by

- floor masses m_L equal to $m_L = \rho_m m$,
- storey lateral stiffnesses k_L equal to $k_L = \rho_k k$

where ρ_m and ρ_k are given in Table 4. For sake of completeness, Table 4 also gives the ratio, ρ_T, between the fundamental period, $T_{1,L}$, of each lateral-resisting element L and the fundamental period, $T_{1,F}$, of the frame structure F.

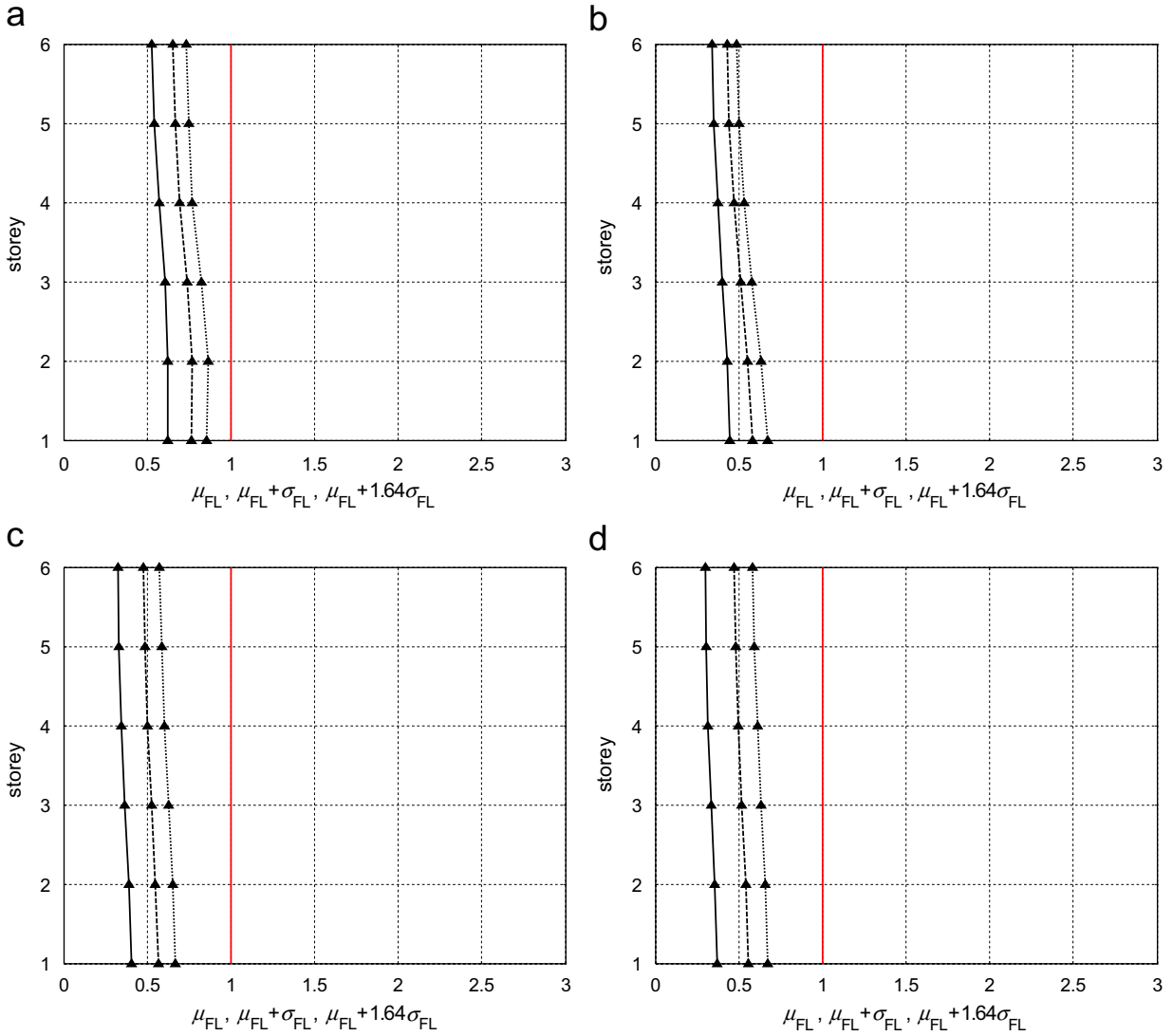

Fig. 40. Profiles of $\mu_{\text{FL-MPD-I}}$ (black continuous line), $\mu_{\text{FL-MPD-I}}+\sigma_{\text{FL-MPD-I}}$ (black dashed line) and $\mu_{\text{FL-MPD-I}}+1.64\sigma_{\text{FL-MPD-I}}$ (black dotted line): (a) L_5, (b) L_6, (c) L_7 and (d) L_8.

The parametric study is carried out for the following dynamic systems (structures + equal "total size" ensemble of additional dampers):

- structural system FL with no added viscous dampers (and null internal damping), referred to as FL-UND dynamic system, as per Fig. 31b;
- structural system FL with the F structure equipped with SPD system, referred to as FL-SPD dynamic system, as per Fig. 32a and Table 2;
- structural system FL with the F structure equipped with MPD system (direct implementation), referred to as FL-MPD dynamic system, as per Fig. 32b and Table 2;
- indirect implementation of the MPD system. The indirect implementation is obtained placing the same dampers of the FL-MPD dynamic system between the corresponding storey of structure F and structure L, as per Fig. 32c and Table 2. This dynamic system will be referred to as FL-MPD-I dynamic system.

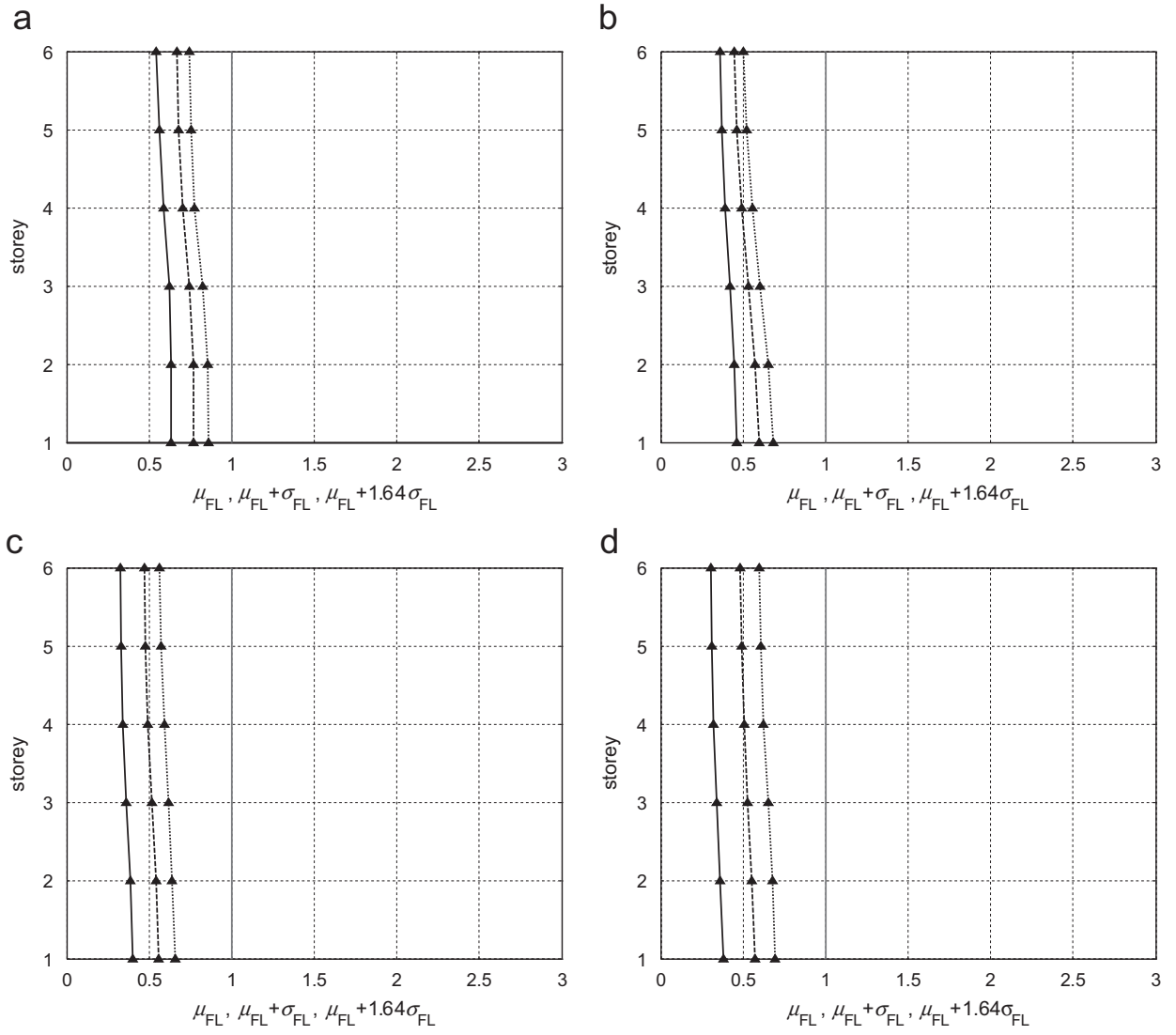

Fig. 41. Profiles of $\mu_{\text{FL-MPD-I}}$ (black continuous line), $\mu_{\text{FL-MPD-I}}+\sigma_{\text{FL-MPD-I}}$ (black dashed line) and $\mu_{\text{FL-MPD-I}}+1.64\sigma_{\text{FL-MPD-I}}$ (black dotted line): (a) L_9, (b) L_{10}, (c) L_{11} and (d) L_{12}.

Note that, due to the equal "total size" constraint and the properties of the structure, each damper of the ensemble of 6 dampers inserted in the FL-SPD, FL-MPD and FL-MPD-I dynamic systems is characterised by a damping coefficient c_j equal to $\bar{c}/6 = 1.5 \times 10^6\,\text{N s/m}$.

The response of the above dynamic systems is numerically computed under the effects of 40 historically recorded earthquake ground motions. Out of these, 30 are far-field records and 10 near-field records; all are scaled to the same PGA value of $0.3g$.

For each earthquake, taking as reference the maximum shear developed by the FL-SPD dynamic system at each ith storey, the following storey response ratios can be computed:

$$(r_i)_{\text{FL-UND}} = \frac{(V_{\max -i})_{\text{FL-UND}}}{(V_{\max -i})_{\text{FL-SPD}}}, \tag{36}$$

$$(r_i)_{\text{FL-MPD}} = \frac{(V_{\max -i})_{\text{FL-MPD}}}{(V_{\max -i})_{\text{FL-SPD}}}, \tag{37}$$

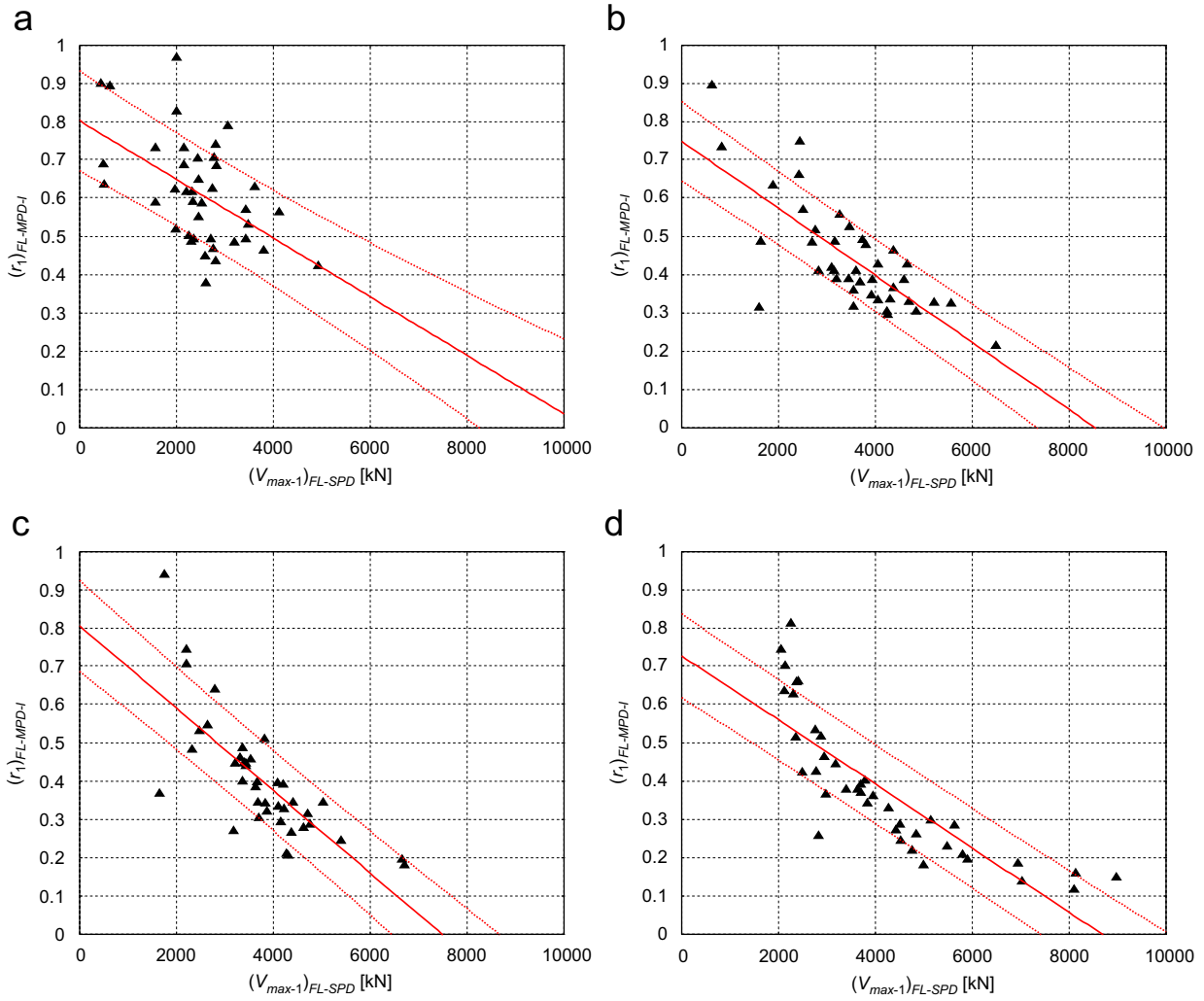

Fig. 42. (▲)Response ratio at the base, $(r_1)_{\text{FL-MPD-I}}$, as a function of the maximum base shear of the FL-SPD system, $(V_{\max -1})_{\text{FL-SPD}}$; (red continuous line) least square fit regression line of the data and (red dotted lines) 50% confidence bounds: (a) L_1, (b) L_2, (c) L_3 and (d) L_4.

$$(r_i)_{\text{FL-MPD-I}} = \frac{(V_{\max -i})_{\text{FL-MPD-I}}}{(V_{\max -i})_{\text{FL-SPD}}}, \tag{38}$$

where $(V_{\max -i})_{\text{FL-UND}}$, $(V_{\max -i})_{\text{FL-SPD}}$, $(V_{\max -i})_{\text{FL-MPD}}$ and $(V_{\max -i})_{\text{FL-MPD-I}}$ denote the maximum shear at the ith storey developed, respectively, by the FL-UND, FL-SPD, FL-MPD and FL-MPD-I dynamic systems.

The means of the response ratios given by Eqs. (36)–(38), for all 40 earthquakes considered, are referred to, respectively, as $\mu_{\text{FL-UND}}$, $\mu_{\text{FL-MPD}}$ and $\mu_{\text{FL-MPD-I}}$. The coefficients of variation of the response ratios given by Eqs. (36)–(38), for all 40 earthquakes considered, are referred to, respectively, as $\text{cov}_{\text{FL-UND}}$, $\text{cov}_{\text{FL-MPD}}$ and $\text{cov}_{\text{FL-MPD-I}}$. The standard deviations of the response ratios given by Eq. (38), for all 40 earthquakes considered, are referred to as $\sigma_{\text{FL-MPD-I}}$.

Figs. 33–35 (Figs. 34 and 35 only available in the online version of this article) show the results (in terms of $\mu_{\text{FL-UND}}$, $\mu_{\text{FL-MPD}}$ and $\mu_{\text{FL-MPD-I}}$) obtained, respectively: in the case of lateral-resisting elements L_1, L_2, L_3 and L_4, in the case of lateral-resisting elements L_5, L_6, L_7 and L_8, and in the case of lateral-resisting elements L_9, L_{10}, L_{11} and L_{12}. Figs. 36–38 (Figs. 37 and 38 only available in the online version of this article) show the results (in terms of $\text{cov}_{\text{FL-UND}}$, $\text{cov}_{\text{FL-MPD}}$ and $\text{cov}_{\text{FL-MPD-I}}$) obtained, respectively: in the case of lateral-resisting elements L_1, L_2, L_3 and L_4, in the case of lateral-resisting elements L_5, L_6, L_7 and L_8, and in the case

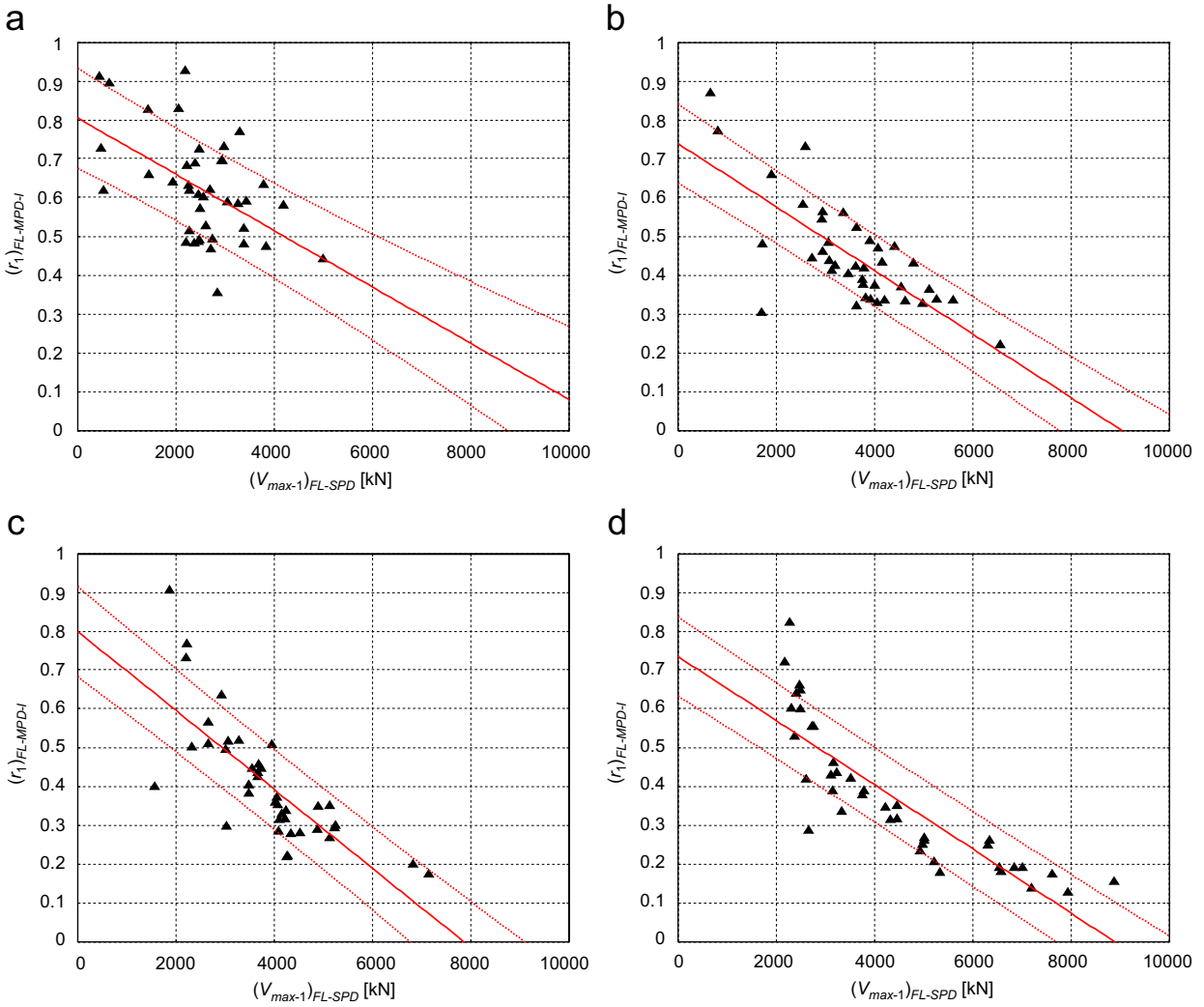

Fig. 43. (▲) Response ratio at the base, $(r_1)_{\text{FL-MPD-I}}$, as a function of the maximum base shear of the FL-SPD system, $(V_{\max -1})_{\text{FL-SPD}}$; (red continuous line) least square fit regression line of the data and (red dotted lines) 50% confidence bounds: (a) L_5, (b) L_6, (c) L_7 and (d) L_8.

of lateral-resisting elements L_9, L_{10}, L_{11} and L_{12}. Figs. 39–41 (Figs. 40 and 41 only available in the online version of this article) show the results (in terms of $\mu_{\text{FL-MPD-I}}$, $\mu_{\text{FL-MPD-I}} + \sigma_{\text{FL-MPD-I}}$ and $\mu_{\text{FL-MPD-I}} + 1.64\sigma_{\text{FL-MPD-I}}$) obtained, respectively: in the case of lateral-resisting elements L_1, L_2, L_3 and L_4, in the case of lateral-resisting elements L_5, L_6, L_7 and L_8, and in the case of lateral-resisting elements L_9, L_{10}, L_{11} and L_{12}.

Inspection of Figs. 33–35 shows that, for all dynamic systems considered, $\mu_{\text{FL-MPD-I}}$ is always substantially smaller than unity and, in most cases, very close to $\mu_{\text{FL-MPD}}$. The coefficients of variation of the response ratios are within the range of 0.2–0.6 for all dynamic systems considered, as given in Figs. 36–38. Figs. 39–41 show that, in all cases, $\mu_{\text{FL-MPD-I}} + 1.64\sigma_{\text{FL-MPD-I}}$ is smaller than unity, thus indicating that, in a statistical interpretation of the results obtained, the probability that $(V_{\max -i})_{\text{FL-MPD-I}}$ is larger than $(V_{\max -i})_{\text{FL-SPD}}$ is very low (less than 5%). It is worth noting that, in the numerical analyses carried out, for all earthquakes and all dynamic systems considered, at each storey, $(V_{\max -i})_{\text{FL-MPD-I}}$ turns out to be always smaller than $(V_{\max -i})_{\text{FL-SPD}}$.

Figs. 42–44 (Figs. 43 and 44 only available in the online version of this article) plot the response ratio at the base, $(r_1)_{\text{FL-MPD-I}}$, as a function of the maximum base shear of the FL-SPD dynamic system, $(V_{\max -1})_{\text{FL-SPD}}$, as well as the least square fit regression line of the data (together with the 50% confidence bounds). Note that,

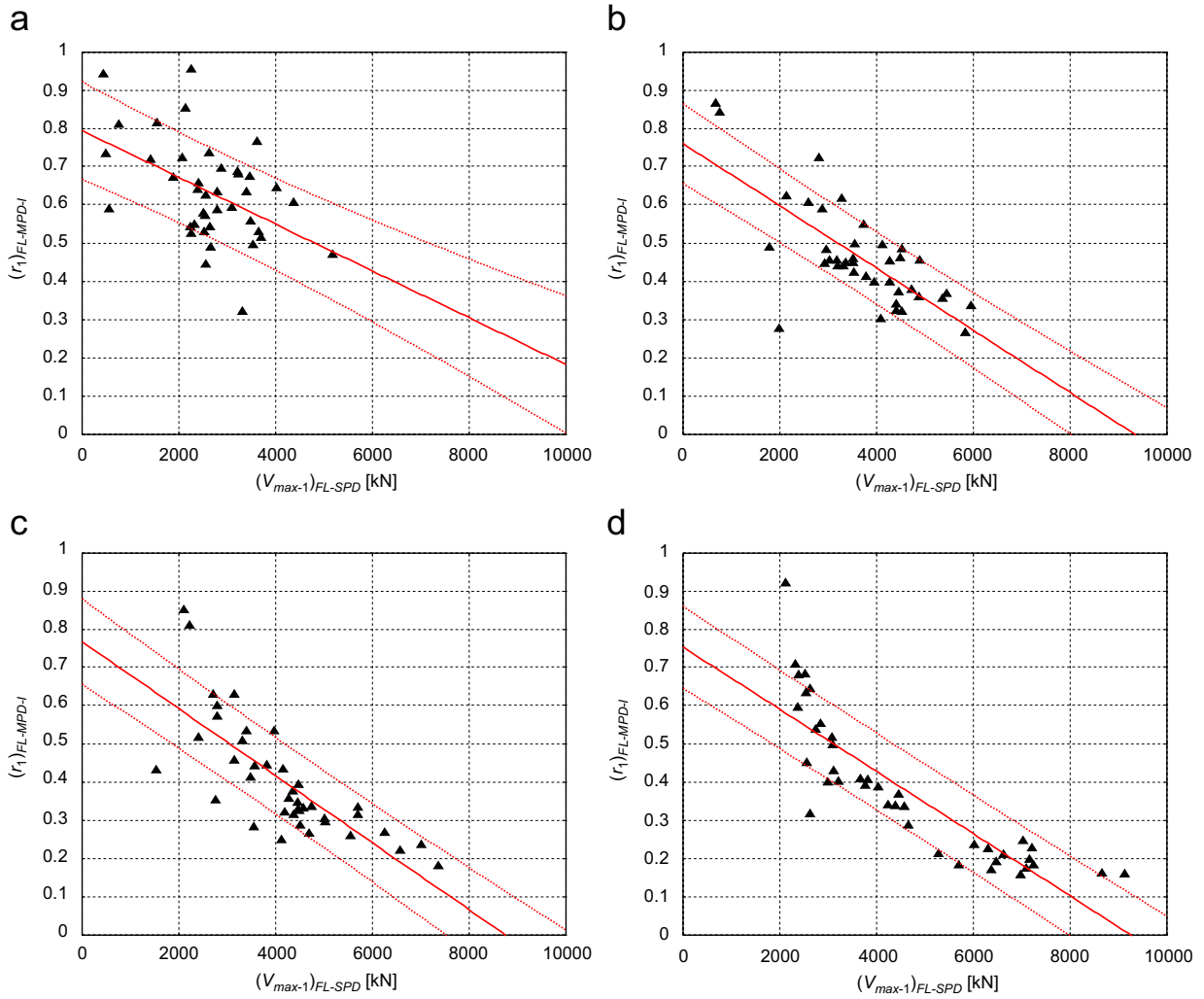

Fig. 44. (▲) Response ratio at the base, $(r_1)_{\text{FL-MPD-I}}$, as a function of the maximum base shear of the FL-SPD system, $(V_{\max -1})_{\text{FL-SPD}}$; (red continuous line) least square fit regression line of the data and (red dotted lines) 50% confidence bounds: (a) L_9, (b) L_{10}, (c) L_{11} and (d) L_{12}.

in all cases, the angular coefficient of the regression line is negative, thus indicating that the response ratio $(r_1)_{\text{FL-MPD-I}}$ decreases with increasing of the total demand imposed by the seismic input upon the structure.

To sum up, the results indicate that the indirect implementation of the MPD system leads to a damping efficiency which is (i) always larger than that provided by the implementation of the equal "total size" SPD system (with the difference between the efficiencies of the two systems becoming larger and larger as the effects of the earthquakes upon the structures become higher and higher) and (ii) very similar to (and, in some cases, larger than) that provided by the direct implementation of the MPD system. This result opens the grounds for a new conceptual design strategy: insertion of dampers between frames and lateral-resisting elements. An illustrative example of such application is provided in a previous work by the authors [12].

8. Conclusions

This paper firstly recalls the fundamental properties of shear-type (either mechanical or structural) systems characterised by a damping matrix proportional to the mass matrix (MPD) pointing out how these systems: (a) display superior dissipative capacities (w.r.t. other systems which satisfy the here defined equal "total size"

constraint) and (b) are made up of dampers which connect each mass to a fixed point and are sized proportionally to the corresponding mass.

Secondly, this paper investigates how such MPD systems can be obtained in actual civil building structures through the use of additional (manufactured) viscous dampers. Two ways of implementing MPD systems are herein identified: direct and indirect implementation. In the direct implementation of MPD systems dampers connect each floor to the ground: this requires the use of bracing systems of large size (with all the issues relative to the buckling phenomena). Nonetheless, few examples of application of such large-sized damper-equipped bracing systems have been recently realised (even though not following an exact MPD system) and are reported herein. In the indirect implementation of MPD systems dampers are placed between two adjacent structures (a reference structure and a "support" structure). Depending on the type of the "support" structure, two cases can be envisaged for this solution: (case 1) insertion of dampers between two adjacent structures characterised by different dynamic properties and (case 2) insertion of dampers between a frame structure and a very stiff lateral-resisting element often present in building structures designed for seismic areas. The parametric studies developed by the authors and here presented indicate that, for case 1, indirect implementation of MPD systems provides a good damping efficiency only if the two adjacent structures are characterised by very different dynamic properties. On the other hand, for case 2, results indicate that, for common building structures, in most cases, indirect implementation of MPD systems leads to good dissipative properties (very similar to those offered by direct implementation of MPD systems). This last result opens new ground for a novel way (between the frames and the lateral-resisting elements) for "optimal" insertion of viscous dampers in building structures.

The findings, even though obtained with specific reference to coupled shear-type structural systems, may give useful insight also into the effective addition of viscous dampers in coupled shear-type mechanical systems.

Acknowledgements

The authors are grateful to Dr. Philippe Duflot of Taylor Devices Europe (for kindly providing information regarding the application of "mega-braces" in the Chapultepec Tower) and to Pr. Stefano Sorace of University of Udine (for kindly allowing the inclusion of picture representing the schematic functioning of the SPIDER dissipative bracing system).

References

[1] G.C. Hart, K. Wong, *Structural Dynamics for Structural Engineers*, Wiley, New York, 2000.
[2] ⟨http://nisee.berkeley.edu/prosys/applications.html⟩.
[3] I. Takewaki, Optimal damper placement for minimum transfer functions, *Earthquake Engineering and Structural Dynamics* 26 (1997) 1113–1124.
[4] I. Takewaki, Optimal damper placement for critical excitation, *Probabilistic Engineering Mechanics* 15 (2000) 317–325.
[5] I. Takewaki, *Dynamic Structural Design: Inverse Problem Approach*, WIT Press, Southampton, SO40 7AA, UK, 2000.
[6] I. Takewaki, S. Yoshitomi, K. Uetani, K. Masaaki, M. Tsuji, Non-monotonic optimal damper placement via steepest direction search, *Earthquake Engineering and Structural Dynamics* 28 (1999) 655–670.
[7] D. Lopez Garcia, A simple method for the design of optimal configurations in MDOF structures, *Earthquake Spectra* 17 (3) (2001) 387–398.
[8] M.P. Singh, L.M. Moreschi, Optimal seismic response control with dampers, *Earthquake Engineering and Structural Dynamics* 30 (2001) 553–572.
[9] M.P. Singh, L.M. Moreschi, Optimal placement of dampers for passive response control, *Earthquake Engineering and Structural Dynamics* 31 (2002) 955–976.
[10] J.A. Main, S. Krenk, Efficiency and tuning of viscous dampers on discrete systems, *Journal of Sound and Vibration* 286 (2005) 97–122.
[11] S. Silvestri, T. Trombetti, C. Ceccoli, Inserting the mass proportional damping (MPD) system in a concrete shear-type structure. *Structural Engineering and Mechanics* 16 (2) (2003) 177–193, ISSN:1225-4568.
[12] T. Trombetti, S. Silvestri, Added viscous dampers in shear-type structures: the effectiveness of mass proportional damping, *Journal of Earthquake Engineering* 8 (2) (2004) 275–313.
[13] T. Trombetti, C. Ceccoli, S. Silvestri, Mass proportional damping as a seismic design solution for an 18-storey concrete-core & steel-frame structure. *Proceedings of the Speciality Conference on "The Conceptual Approach to Structural Design"*, Singapore, 29–30 August 2001.

[14] T. Trombetti, S. Silvestri, C. Ceccoli, Inserting viscous dampers in shear-type structures: numerical investigation of the MPD system performances, *Proceedings of "The Second International Conference on Advances in Structural Engineering and Mechanics"* (ASEM'02), Busan, Korea, August 2002.
[15] S. Silvestri, T. Trombetti, C. Ceccoli, An innovative damping scheme for shear-type structures: the MPD system, *Proceedings of "The 2nd International Speciality Conference on The Conceptual Approach to Structural Design"*, Vol. 2, CDS-03, Milano Bicocca, Italy, July 2003, pp. 789–796, ISBN:981-04-8561-1.
[16] S. Silvestri, T. Trombetti, Optimal insertion of viscous dampers into shear-type structures: dissipative properties of the MPD system, *Proceedings of the "13th World Conference on Earthquake Engineering"*, 13WCEE, Vancouver, BC, Paper No. 473, Canada, August 1–6, 2004.
[17] T. Trombetti, S. Silvestri, On the modal damping ratios of shear-type structures equipped with Rayleigh damping systems, *Journal of Sound and Vibration* 292 (2006) 21–58.
[18] A.K. Chopra, *Dynamics of Structures. Theory and Applications to Earthquake Engineering*, Prentice-Hall, Upper Saddle River, NJ, 1995.
[19] S.H. Crandall, W.D. Mark, *Random Vibrations in Mechanical Systems*, Academic Press, New York, London, 1963.
[20] J.H. Holland, *Adaptation in Natural and Artificial Systems*, University of Michigan Press, Ann Arbor, MI, 1975.
[21] L. Davis, *Genetic Algorithms and Simulated Annealing*, Morgan Kaufmann, Los Altos, CA, 1987.
[22] L. Davis, *Handbook of Genetic Algorithms*, Van Nostrand Reinhold, New York, 1991.
[23] J.H. Holland, Genetic algorithms. *Scientific American* (1992) 44–50.
[24] M. Gen, R. Cheng, *Genetic Algorithms and Engineering Design*, Wiley, New York, 1997.
[25] A.J. Keane, Passive vibration control via unusual geometries: the application of genetic algorithm optimisation to structural design, *Journal of Sound and Vibration* 185 (3) (1995) 441–453.
[26] I.I. Esat, H. Bahai, Vibratory system synthesis for multi-body systems based on genetic algorithm, *Journal of Sound and Vibration* 230 (4) (2000) 933–948.
[27] P.W. Clark, I.D. Aiken, E. Ko, K. Kasai, I. Kimura, Design procedures for building incorporating hysteretic damping devices, *Proceedings of the 68th Annual Convention, Structural Engineers Association of California*, Santa Barbara, CA, 1999.
[28] 〈http://www.arup.com/dyna/applications/seismic/seismic.htm〉.
[29] P. Brown, I.D. Aiken, F.J. Jafarzadeh, Seismic Retrofit of the W. F. Bennett Federal Building, *Modern Steel Construction*, 2001 〈http://www.aisc.org/msc/0108_03_seismicretrofit.pdf〉.
[30] A. Chiarugi, G. Terenzi, S. Sorace, Metodo di progetto di dispositivi siliconici per l'isolamento alla base: applicazione a due casi sperimentali. *Atti del 10° Convegno Nazionale ANIDIS*, Potenza-Matera, Italy, September 2001.
[31] J.E. Luco, F.C.P. De Barros, Optimal damping between two adjacent elastic structures, *Earthquake Engineering and Structural Dynamics* 27 (1998) 649–659.
[32] W.S. Zhang, Y.L. Xu, Dynamic characteristics and seismic response of adjacent buildings linked by discrete dampers, *Earthquake Engineering and Structural Dynamics* 28 (1999) 1163–1185.
[33] Y.L. Xu, S. Zhan, J.M. Ko, W.S. Zhang, Experimental investigation of adjacent buildings connected by fluid damper, *Earthquake Engineering and Structural Dynamics* 28 (1999) 609–631.
[34] Y.L. Xu, W.S. Zhang, Modal analysis and seismic response of steel frames with connection dampers, *Engineering Structures* 23 (2001) 385–396.
[35] W.S. Zhang, Y.L. Xu, Vibration analysis of two buildings linked by Maxwell model-defined fluid dampers, *Journal of Sound and Vibration* 233 (5) (2000) 775–796.
[36] Y.Q. Ni, J.M. Ko, Random seismic response analysis of adjacent buildings coupled with non linear hysteretic dampers, *Journal of Sound and Vibration* 246 (3) (2001) 403–417.
[37] T. Aida, T. Aso, K. Takeshita, T. Takiuchi, T. Fujii, Improvement of the structure damping performance by interconnection, *Journal of Sound and Vibration* 242 (2) (2001) 333–353.